PERFORMANCE OF PAIRS TRADING STRATEGIES BASED ON RENKO AND KAGI CHARTS

YUFEI SUN

UNIVERSITY OF WARSAW
FACULTY OF ECONOMIC SCIENCES

WORKING PAPERS

Performance of Pairs Trading Strategies Based on Renko and Kagi Charts

Yufei Sun[1]*

[1]Faculty of Economic Sciences, University of Warsaw
*Corresponding authors: y.sun2@uw.edu.pl

Abstract: This paper investigates the profitability and robustness of pairs trading strategies based on non-parametric technical chart constructions—Renko and Kagi—across the U.S. and Chinese equity markets. Within a market-neutral, mean-reversion framework, the study examines strategy performance under varying market regimes, including the Global Financial Crisis (GFC) and the COVID-19 period. Using historical data from indices such as the S&P 500 and the CSI series, pairs are selected via statistical patterns in Renko and Kagi charts. Robustness checks consider varying trading horizons, the number of pairs, and transaction costs. Results show that both chart-based strategies generate significant excess returns and exhibit strong Sharpe ratios before costs. While trading frictions reduce profitability, Renko-based strategies remain resilient, especially during crises. The findings highlight that adaptive and non-parametric charting methods can effectively capture transient mispricings and provide viable alternatives for statistical arbitrage in turbulent markets.

1. Introduction

Pairs trading, a well-known quantitative strategy that has been widely used since the 1990s, attracts both institutional and individual investors due to its market-neutral approach and potential for consistent, low-volatility returns. The strategy typically produces small but steady profits and has been extensively studied in the literature, with seminal works by Herlemont (2003), Vidyamurthy (2004), Elliott et al. (2005), Do et al. (2006), and Gatev et al. (2006) laying its theoretical and empirical foundations.

The core principle of pairs trading consists of three steps. First, a pair of assets is identified based on historically correlated price movements. Second, when their prices diverge, the overperforming asset ("winner") is shorted while the underperforming asset ("loser") is bought. Finally, both positions are unwound once prices realign, thereby capturing the convergence profit.

Despite numerous variations of the strategy, they all rest on the same premise: the prices of the paired assets will eventually converge. In practice, three operational challenges must be resolved before any trade is initiated: (i) selecting the pairs, (ii) determining entry points, and (iii) defining exit points. Traditional approaches address these challenges by estimating a time-varying "fair value" of the spread and trading on the expectation of reversion toward this benchmark. However, during crises or structural shifts, the fair value itself may drift, generating false signals and undermining profitability.

Across the literature, methods of pair formation and trade execution vary, but all rely on the concept of equilibrium in prices or returns: two related assets are expected to yield comparable returns over time. Deviations from this equilibrium are often attributed to market overreactions, underreactions to new information, or mispricing. The fundamental assumption of pairs trading is that such deviations are temporary and will eventually self-correct.

This equilibrium concept is closely linked to cointegration theory (Engle and Granger, 1991), which posits that the spread between cointegrated assets should exhibit mean-reverting behavior. In theory, when the spread deviates from its long-term mean, it is expected to revert.

In practice, however, mean reversion is not guaranteed. Asset-specific shocks such as news or events may alter the characteristics of the spread, shifting it away from its historical mean. These shifts may result in longer recovery times—possibly beyond the planned investment

horizon—or, in some cases, prevent reversion altogether. Consequently, relying solely on equilibrium-based assumptions may render pairs trading ineffective. Empirical evidence (Do and Faff, 2010) supports this concern, showing that returns often diminish once transaction costs are accounted for.

Two main approaches attempt to address the problem of a drifting mean. The first replaces the long-term mean with a fixed-length moving average (MA). Although widely used by practitioners, MA-based methods suffer from delayed responses due to inherent lag. The second relies on regime-switching models (Wu and Elliott, 2005; Bock and Mestel, 2009; Endres and Stübinger, 2019), where the mean is allowed to shift between regimes. While this improves adaptability in theory, empirical applications remain limited, and it is unclear whether such shifts can be detected and exploited quickly enough in practice.

We propose a non-parametric approach to pairs trading that leverages statistical characteristics of the spread process, as outlined in Bogomolov (2013). Unlike traditional methods, this approach does not estimate or track the mean but instead relies on the relative stability of spread variability over time. The intuition is straightforward: the likelihood of reversal increases as prices deviate further from equilibrium. The challenge lies in defining a threshold beyond which a contrarian trade becomes favorable, with spread variability being the key determinant. Figure 1 illustrates the idea of stable variability alongside uncertainty in the exact mean location.

The method used to assess the variability of the spread process in this study builds on the Renko and Kagi chart constructions, first introduced into academic research by Pastukhov (2005). Originating in 19th-century Japan, Renko and Kagi charts are widely recognized in technical analysis within financial markets. They focus exclusively on price movements that exceed a predefined threshold, while deliberately omitting information on time and trading volumes. This design aims to filter out minor fluctuations, or "trading noise," thereby capturing only meaningful price dynamics.

Pastukhov's work provided a rigorous mathematical foundation for Renko and Kagi constructions, highlighting their potential to generate trading strategies based on the statistical properties of these charts. While his research concentrated on single-asset prices, we extend the framework to spread processes in pairs trading. In this paper, Renko and Kagi constructions are

employed not only for individual assets but also to identify and evaluate pairs trading opportunities, particularly under the Ornstein–Uhlenbeck (OU) process specification. We theoretically validate the effectiveness of this approach and further apply it to real market data from the U.S. and Chinese stock exchanges.

This study fills an important gap and makes four concrete contributions.

1. First, I introduce a methodological extension by being among the first to formulate Renko/Kagi H-constructions specifically for spread processes and to derive their properties under an OU specification.

2. Second, I establish a closed-form profitability condition: if the chart-implied H-volatility σ_H satisfies $\sigma_H < H$, then a simple contrarian H-strategy yields a positive expected return under an OU spread. This result provides a direct link between technical thresholds and the underlying statistical parameters.

3. Third, I conduct comprehensive empirical tests using daily equity data from 1995 to 2024, covering both U.S. (S&P 500) and Chinese (four CSI indices) markets. The evaluation includes stress periods such as the GFC and the COVID-19 pandemic, as well as multiple transaction-cost regimes, thereby ensuring robustness. Our results show that Renko-based strategies remain profitable even when classical distance or cointegration rules fail, particularly during volatile regimes such as the GFC and COVID-19 periods. This suggests that volatility-centric thresholds can complement— or, in stressed markets, even replace—mean-reversion signals widely employed by hedge funds and proprietary desks.

4. Fourth, I provide a practical implementation guide. Specifically, I propose a data-driven method for selecting the threshold H based on observed spread variability and trading costs, and I demonstrate that portfolio diversification across 5 to 50 pairs significantly enhances the information ratio.

Overall, our results indicate that Renko-based strategies remain robust and profitable, especially in turbulent market environments, such as the GFC and COVID-19 periods.

The structure of this paper is as follows: Section 2 provides a brief overview of Pastukhov's Renko and Kagi methods, their properties, applications to the Wiener process, and the two trading strategies they enable. Section 3 examines the application of Renko and Kagi constructions to the OU process and discrete-time processes. Section 4 details the practical implementation of the proposed pairs trading strategy and describes its testing on real market

data. Section 5 presents the empirical results, and Section 6 concludes the paper with a summary of findings.

Figure 1. Daily log-price spread process with 60-day moving average and 10% bands.
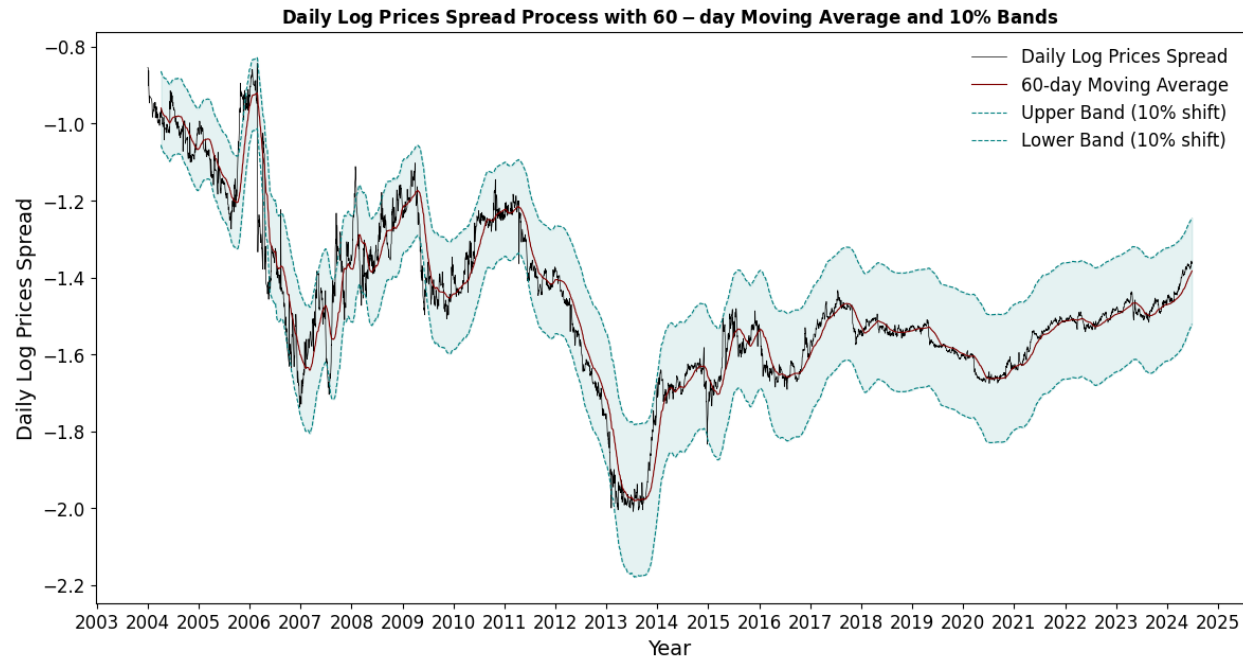
Note: This figure shows daily log prices spread process between two major Chinese banks–Huaxia Bank (600015.SH) and China Minsheng Bank (600016.SH). The red line is the 60-day moving average and the blue lines are the same moving average shifted 10% up and down from its true location.

2. Overview of Renko and Kagi Methods

2.1 Renko Construction

The Renko chart is a Japanese charting technique that emphasizes significant price movements by filtering out minor fluctuations, thereby providing a clearer view of underlying trends. Unlike traditional time-based charts, Renko charts are constructed solely on the basis of price changes exceeding a fixed magnitude, referred to as the brick size. This allows for the identification of key support and resistance levels, as well as potential trend reversals.

Let P(t) denote a continuous price process or cumulative return over the interval [0, T]. The Renko construction discretizes this continuous path into a sequence of movements of fixed size $H > 0$, effectively capturing meaningful trends while discarding noise.

To construct the Renko chart, we define a sequence of increasing time points $\{s_i\}_{i=0}^N$, where $s_0 = 0$ and $s_N \leq T$. These time points are determined based on a predefined threshold $H > 0$, which represents the minimum price movement considered significant. The value of H should satisfy the condition:

$$H \leq \max_{t\in[0,T]} P(t) - \min_{t\in[0,T]} P(t) \tag{1}$$

The sequence $\{s_i\}$ is constructed recursively using the following rule:

$$s_i = \inf\{u \in [s_{i-1}, T]: |P_{(u)} - P_{(s_{i-1})}| = H\}, i = 1,2,\dots,N \tag{2}$$

This is, s_i is the earliest time after s_{i-1} when the price process $P(t)$ has moved by exactly H from its value at time s_{i-1}. The process $X(i) = P(s_i)$ for $i = 0,1,\dots,N$ forms the Renko process, which can be visualized as a sequence of "bricks" in the Renko chart, as shown in Figure 2, each representing a price movement of size H.

In the statistical framework, the Renko construction is closely related to the notions of H-fluctuation and Renko-H-inversion, as introduced by Pastukhov (2005). The H-fluctuation $U_T(H,P)$ of the process $P(t)$ over the interval [0, T] is defined as:

$$U_T(H,P) = \sup_{T_1} \sum_{k=1}^K |P(t_k) - P(t_{k-1})| \tag{3}$$

where T_1 is the set of all finite partitions $(t_0, t_1, \dots, t_K)$ such that $0 = t_0 < t_1 < \cdots < t_K \leq T$ and $|P(t_k) - P(t_{k-1})| = H$ for $k = 1,\dots,K$. Essentially, the H-fluctuation $U_T(H,P)$ measures the total significant movement of the price process by summing all increments of size H.

The Renko-H-inversion $M_T(H,P)$ corresponds to the maximum number of bricks (i.e., significant moves of size H) that can be extracted from the process:

$$M_T(H,P) = \max\{K \in \mathbf{N}: U_T(H,P) = KH\} \tag{4}$$

This variable reflects the frequency of significant price changes within [0, T] and thus serves as a natural estimator for market volatility.

To identify local maxima and minima in the Renko process, two sequences of time points are introduced: $\{s_n^a\}$ for local extrema, and $\{s_n^b\}$ for stopping times corresponding to trend reversals. Their construction is as follows:

1. Initialize $s_0^a = s_0$ and $s_0^b = s_1$.
2. For $n \geq 1$, define s_n^b as the earliest time s_i after s_{n-1}^b where the Renko process changes direction:

$$s_n^b = min\{s_i \geq s_{n-1}^b : (P(s_i) - P(s_{i-1}))(P(s_{i-1}) - P(s_{i-2})) < 0\} \tag{5}$$

3. Once s_n^b is determined, s_n^a is set to the previous time point:

$$s_n^a = s_{i-1}, \ where \ s_n^b = s_i \tag{6}$$

Here, s_n^a marks the time just before a change in direction, corresponding to a local extremum, while s_n^b denotes the time when the reversal is confirmed. Note that in special cases, s_n^b and s_{n+1}^a may coincide if the process reverses immediately in consecutive steps.

These sequences satisfy the following certain mathematical properties:

1. Ordering: $s_n^a < s_n^b \leq s_{n+1}^a$, $\forall n = 0,1, \dots, M$.
2. Threshold Condition: $|P(s_n^a) - P(s_n^b)| = H$, $\forall n = 0,1, \dots, M$.
3. Alternation of Trend Direction: $sign(P(s_n^a) - P(s_{n-1}^a)) = (-1)^n sign(P(s_1^a) - P(s_0^a))$, $\forall n \geq 1$.

These conditions ensure that the Renko chart accurately reflects significant price changes and trend reversals.

The Renko construction effectively filters out minor price movements and emphasizes significant trends by only recording price changes of at least H. This makes it a valuable tool for identifying support and resistance levels, as well as for detecting potential entry and exit points in trading strategies.

By analyzing the Renko chart, one can compute the Renko-H-volatility $\xi_T(H, P)$, defined as:

$$\xi_T(H, P) = \frac{U_T(H,P)}{M_T(H,P)} \tag{7}$$

For the Renko process, since each brick corresponds to a fixed price movement of size H, the Renko-H-volatility is simply H. However, when analyzing higher-order volatilities or stochastic processes such as the Wiener process, this quantity offers valuable insights into price variability and facilitates comparisons between empirical data and theoretical models.

In addition, the Renko construction enables the design of trading strategies that exploit systematic patterns in price dynamics. By quantifying both the frequency and cumulative effect of significant price moves, traders can evaluate market efficiency and identify potential arbitrage opportunities. The Renko-H-inversion $M_T(H, P)$ serves as a practical estimator of market volatility, reflecting the intensity of meaningful fluctuations.

The choice of H plays a central role in the Renko framework. A smaller H produces a more sensitive chart that captures a larger number of price movements, including relatively minor fluctuations. While this may benefit short-term traders, it also introduces additional noise. Conversely, a larger H filters out minor variations and highlights long-term trends, which can be more suitable for longer investment horizons but risks overlooking short-lived opportunities. The optimal value of H therefore depends on the underlying asset's volatility, the trader's time horizon, and the trading strategy applied.

For illustration, consider a price series $P(t)$ over the interval [0, T] with $H = 1$. Starting from $s_0 = 0$, we identify s_1 as the first time $t \geq s_0$ when $| P(t) - P(s_0) | = 1$. Proceeding similarly, we obtain s_2, s_3, …. If $P(s_1) - P(s_0) > 0$ and $P(s_2) - P(s_1) < 0$, then a reversal occurs at $s_1^b = s_2$ identified as a local maximum, as illustrated in Figure 3.

In summary, the Renko chart reduces the complexity of price dynamics by focusing exclusively on significant movements. This makes it particularly valuable in statistical arbitrage—such as pairs trading—where identifying meaningful deviations is critical. By leveraging Renko-derived statistics such as M_T and ξ_T, traders can formulate robust volatility-based trading rules that remain resilient to structural breaks and market microstructure noise.

Figure 2. Renko charts for the asset price process and the corresponding Renko transformation.
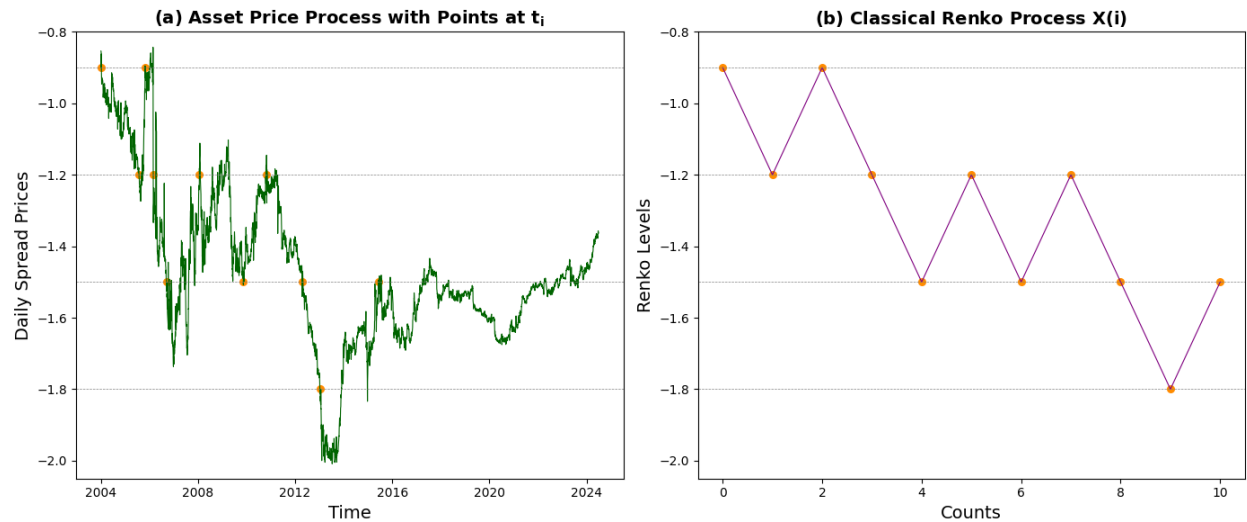
Note: Panel (a) illustrates the asset price process $P(t)$, where the orange markers highlight time points t_i corresponding to threshold-exceeding movements. Panel (b) shows the associated Renko process $X(i)$, where each brick represents a movement of at least $H = 0.3$. Dashed gray lines are added as visual references for the threshold levels applied in both panels.

Figure 3. Renko construction with identified stopping times and local extrema.
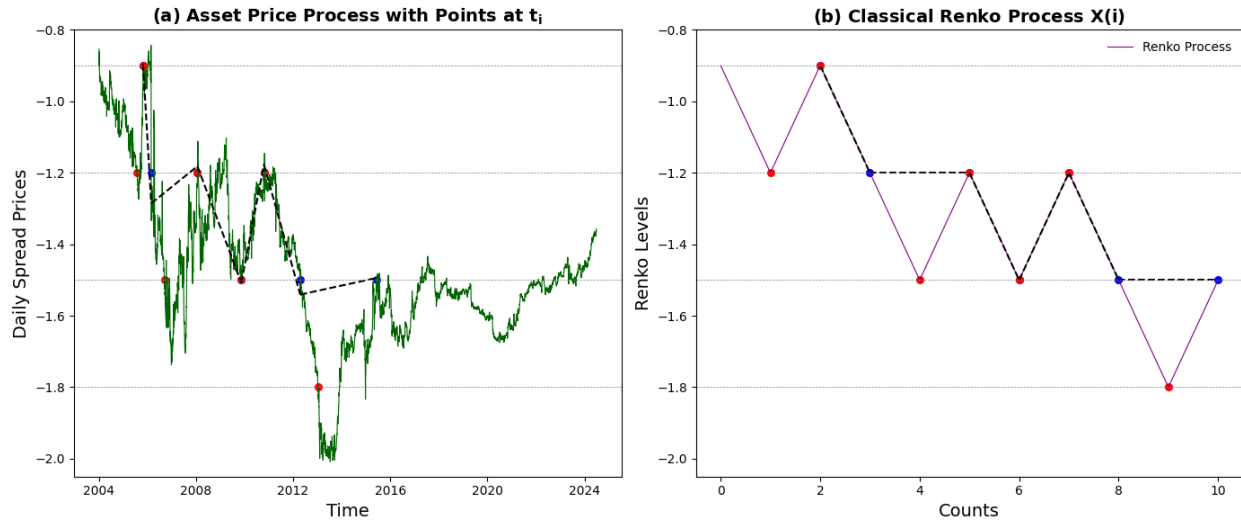
Note: anel (a) depicts the asset price process $P(t)$, where blue markers indicate stopping times S_n^b and red markers highlight local extrema S_n^a, corresponding to significant reversals. Black dotted lines connect consecutive stopping times to illustrate trading intervals. Panel (b) presents the Renko process $X(i)$, where red markers denote local extrema and blue markers represent stopping times. Dashed gray lines indicate the threshold level $H = 0.3$, consistently applied across both panels.

2.2 Kagi Construction

The Kagi chart is a Japanese charting technique designed to capture major price reversals and trend continuations by filtering out insignificant fluctuations. While both Kagi and Renko charts simplify raw price movements, they differ fundamentally in construction and application. The Renko chart discretizes price changes into uniform bricks of fixed size and operates on a derived process. In contrast, the Kagi chart works directly with the actual price path $P(t)$, allowing it to reflect not only the magnitude but also the timing and sequence of real price reversals.

This distinction makes Kagi charts particularly well-suited for identifying structural changes in market sentiment and momentum. Since the construction depends on sequential highs and lows in the real price series, the Kagi chart can more accurately capture dynamics such as breakout confirmations, support/resistance violations, and reversal strength.

Let $P(t)$ be a continuous time series representing the actual asset prices or cumulative returns over the interval $[0, T]$. We define a threshold $H > 0$ that satisfies the condition:

$$H \leq \max_{t \in [0,T]} P(t) - \min_{t \in [0,T]} P(t) \tag{8}$$

The construction involves generating two sequences of time points, $\{s_n^a\}$ and $\{s_n^b\}$. Here, s_n^a denotes the times when the process $P(t)$ reaches a new local maximum or minimum relative to the preceding confirmed extremum, while s_n^b represents the confirmation points at which such extrema are validated by a subsequent price movement of at least H.

The construction begins by identifying the first significant price movement where the cumulative price range reaches the threshold H. Specifically, we define

$$s_0^b = \inf \{u \in [0,T] : \max_{t \in [0,u]} P(t) - \min_{t \in [0,u]} P(t) \geq H\} \tag{9}$$

Then, depending on whether $P(s_0^b)$ is a local maximum or minimum, we define:

$$s_0^a = \begin{cases} \arg \min_{t \in [0,s_0^b]} P(t), & if \ P(s_0^b) = \max_{t \in [0,s_0^b]} P(t) \\ \arg \max_{t \in [0,s_0^b]} P(t), & if \ P(s_0^b) = \min_{t \in [0,s_0^b]} P(t) \end{cases} \tag{10}$$

The initial trend direction is determined by the sign:

$$S_0 = sign(P(s_0^a) - P(s_0^b)) \tag{11}$$

where $S_0 = 1$ indicates that s_0^a is a local maximum, and $S_0 = -1$ indicates a local minimum.

For $n \geq 1$, I recursively define (s_n^a, s_n^b) and S_n, alternating between identifying local maxima and minima based on the previous extremum. If at time s_{n-1}^a I have a local maximum $(S_{n-1} = +1)$, I search for the next significant decline. Specifically, I find s_n^b as:

$$s_n^b = \inf \{u \in [s_{n-1}^a, T] : P(s_{n-1}^a) - \min_{t \in [s_{n-1}^a, u]} P(t) \geq H\} \tag{12}$$

and then identify the new local minimum, $s_n^a = \arg \min_{t \in [s_{n-1}^a, s_n^b]} P(t)$, setting $S_n = -1$.

If at time s_{n-1}^a we have a local minimum $(S_{n-1} = -1)$, we look for the next significant rise:

$$s_n^b = \inf \{u \in [s_{n-1}^a, T] : \max_{t \in [s_{n-1}^a, u]} P(t) - P(s_{n-1}^a) \geq H\} \tag{13}$$

and then identify the new local maximum, $s_n^a = \arg \max_{t \in [s_{n-1}^a, s_n^b]} P(t)$, setting $S_n = +1$.

This alternating process continues until the end of the time interval [0, T] is reached or no further significant movements are detected. The sequences $\{s_n^a\}$ and $\{s_n^b\}$ constructed in the Kagi chart have specific mathematical properties. Firstly, the time points are ordered such that $s_n^a <$

$s_n^b \leq s_{n+1}^a$ for all $n \geq 0$. Secondly, the threshold condition $|P(s_n^b) - P(s_{n-1}^a)| \geq H$ holds for all $n \geq 0$. Thirdly, the trend direction alternates between $S_n = +1$ and $S_n = -1$ for each successive n, and the sign of the price differences satisfies $sign(P(s_n^a) - P(s_{n-1}^a)) = (-1)^n S_0$ for all $n \geq 1$.

The Kagi construction is closely related to the concepts of H-variation and kagi-H-inversion introduced by Pastukhov (2005). The H-variation $V_T(H, P)$ of the process $P(t)$ over the interval [0, T] is defined as:

$$V_T(H, P) = \sup_{T_2} \sum_{l=1}^{L} |P(t_l) - P(t_{l-1})| \tag{14}$$

where T_2 is the set of all finite partitions $(t_0, t_1, \ldots, t_L)$ such that $0 \leq t_0 < t_1 < \cdots < t_L \leq T$ and $|P(t_l) - P(t_{l-1})| \geq H$ for $l = 1, \ldots, L$.

The kagi-H-inversion $N_T(H, P)$ is defined as the number of times the price process $P(t)$ changes direction by at least H over the interval [0, T]. In the Kagi construction, this corresponds directly to the number of sign changes in the sequence $\{S_n\}$.

By analyzing the Kagi chart, one can compute $V_T(H, P)$ and $N_T(H, P)$, which offer quantitative insights into the volatility and directional dynamics of the process $P(t)$. These measures are useful for both developing trading strategies and conducting statistical analysis of financial time series.

To illustrate the Kagi construction, consider a simplified price series $P(t)$ over the interval [0, T] with $H = 1$. Suppose the initial price is $P(0) = 10$. The price reaches $P(t) = 11$ at $t = s_0^b$, where the price range $\max_{t \in [0, s_0^b]} P(t) - \min_{t \in [0, s_0^b]} P(t) \geq 1$. Since $P(s_0^b) = \max_{t \in [0, s_0^b]} P(t)$, we set $s_0^a = \arg \min_{t \in [0, s_0^b]} P(t) = 0$. The initial trend direction is $S_0 = sign\left(P(s_0^a) - P(s_0^b)\right) = sign(10 - 11) = -1$, indicating a starting local minimum.

Since $S_0 = -1$, we look for the next significant rise. The price increases to $P(t) = 12$ at $t = s_1^b$, satisfying $\max_{t \in [s_1^a, s_1^b]} P(t) - P(s_0^a) = 2 \geq H$. We identify $s_1^a = s_1^b$ as the new local maximum and set $S_1 = 1$. The process continues, alternately identifying significant rises and declines based on the threshold H.

In a Kagi chart, vertical lines represent price movements of magnitude at least H, connecting successive local extrema. A change in line direction occurs when the price reverses by at least H from the last extremum. In addition, line thickness or color is often employed to indicate trend direction: for example, a thin line may represent a downward (bearish) phase, while a thick line may indicate an upward (bullish) phase.

Trading signals can be extracted from these structural features. A change in direction indicates a potential reversal and may serve as a buy or sell signal. Horizontal levels corresponding to past reversals act as support or resistance zones for future price movements. Furthermore, when the price surpasses a previous extremum by at least H, it often suggests a continuation of the prevailing trend.

The choice of the threshold H plays a critical role. A smaller H captures more frequent reversals and short-term fluctuations, but it introduces greater noise. A larger H filters out minor variations and highlights long-term dynamics, but may miss short-lived trading opportunities. Hence, the optimal H depends on the asset's volatility, the trader's horizon, and prevailing market conditions.

Importantly, the Kagi construction is not merely a charting tool but also connects to statistical concepts in technical analysis. The number of significant reversals corresponds to the kagi-H-inversion, while the cumulative price variation above the threshold is quantified by the H-variation. These quantities provide statistical measures of volatility, facilitate the development of systematic trading strategies, and contribute to the assessment of market efficiency.

By employing the Kagi construction, traders can reduce complex price trajectories to an interpretable form, highlighting essential reversals and trend continuations. This approach filters out market noise and offers a clearer representation of the underlying price dynamics over time.

2.3 Statistical Properties of Renko and Kagi Constructions

While the Renko and Kagi constructions differ in methodology, they share several statistical properties that shed light on the behavior of financial time series. These properties are central to understanding asset price dynamics and form the basis for robust trading strategies. In

particular, their asymptotic behavior offers theoretical benchmarks for financial modeling and risk management.

A key aspect is the behavior of the H-volatility $v_T(H, P)$ and the H-inversion $N_T(H, P)$ as the observation horizon $T \to \infty$. The former captures the average magnitude of significant price moves, while the latter measures the frequency of trend reversals. Pastukhov (2005) analyzed these properties for the Wiener process $W(t)$, a canonical model for asset prices due to its continuous paths and Gaussian increments.

For the Wiener process scaled by volatility σ, denoted $\sigma W(t)$, Pastukhov demonstrated that the H-volatility of order p converges to a constant multiple of $(\sigma H)^p$ as $T \to \infty$:

$$\lim_{T\to\infty} v_T^{(p)}(H, \sigma W) = R_W(p)(\sigma H)^p \tag{15}$$

where the constant $R_W(p)$ depends on the order p and the type of construction (Renko or Kagi). Specifically, for the Renko construction, the constant $R_W(p)$ is given by:

$$R_W(p) = \sum_{n=1}^{\infty} \frac{n^p}{2^n} \tag{16}$$

which follows from the discrete brick structure and its connection to the geometric distribution. For the Kagi chart, the corresponding constant has an integral representation:

$$R_W(p) = \int_0^{\infty} (1+x)^p e^{-x} dx \tag{17}$$

In the special $p = 1$, both constructions yield $R_W(1) = 2$, leading to the conclusion:

$$\lim_{T\to\infty} v_T(H, \sigma W) = 2\sigma H \tag{18}$$

This implies that, asymptotically, the average significant price movement per reversal is proportional to the product of volatility σ and the threshold H. The factor of 2 reflects the symmetry of the Wiener process, where upward and downward excursions of any given size are equally likely.

These results highlight the self-similarity of the Wiener process and provide theoretical benchmarks against which empirical data can be compared. In practical terms, they suggest that Renko- and Kagi-based measures of volatility converge to universal constants under Brownian dynamics, thereby offering a statistically grounded approach to modeling financial time series.

Furthermore, the H-inversion $N_T(H, \sigma W)$, representing the number of times the price process changes direction by at least H, also exhibits well-defined asymptotic properties. As $T \to \infty$, the expected number of H-inversions grows linearly with time, and satisfies:

$$\lim_{T \to \infty} \frac{N_T(H, \sigma W)}{T} = \frac{1}{E[\tau(H, \sigma W)]} \tag{19}$$

where $E[\tau(H, \sigma W)]$ denotes the expected waiting time between consecutive H-inversions. For the Wiener process, the first hitting time of the levels $\pm H$ has expectation $E[\tau(H, \sigma W)] = H^2/\sigma^2$, yielding the explicit relation:

$$\lim_{T \to \infty} \frac{N_T(H, \sigma W)}{T} = \frac{H^2}{\sigma^2} \tag{20}$$

The asymptotic properties of H-volatility and H-inversion have important implications for financial modeling. The convergence of H-volatility to $2\sigma H$ provides a practical method for estimating the underlying volatility parameter. Specifically, by averaging the magnitude of significant price moves of size H over a sufficiently long horizon, one may obtain:

$$\sigma \approx v_T(H, P)/(2H) \tag{21}$$

This approach is particularly useful when price dynamics resemble a Wiener process or when standard volatility estimators perform poorly in the presence of market anomalies.

The H-inversion $N_T(H, P)$, in turn, serves as a diagnostic of market conditions. A higher frequency of inversions indicates a more volatile, range-bound market, where short-lived reversals dominate. Conversely, fewer inversions imply sustained directional trends, which can be favorable for trend-following strategies such as momentum trading. Monitoring the evolution of H-inversions thus allows traders to adjust their positions dynamically in response to prevailing market regimes.

The dependence of H-volatility on H and σ reflects intrinsic scaling laws in financial time series. In fractal and multifractal analysis, such scaling behaviors are employed to characterize the complexity and self-similarity of market dynamics. The consistent relationship between H-volatility and the threshold H across different scales supports the use of fractal models in finance, offering a theoretical framework to interpret market irregularities and anomalies.

Beyond their theoretical significance, the statistical properties of Renko and Kagi constructions have direct practical applications in trading strategy design. By exploiting the

insights provided by H-volatility and H-inversion, traders can improve decision-making and enhance risk management practices. A critical consideration is the selection of the threshold H, which governs the trade-off between sensitivity and noise. A smaller H captures more frequent but smaller movements, making the chart highly responsive to short-term fluctuations but prone to false signals. Conversely, a larger H filters out minor noise and emphasizes major price changes, though at the cost of delayed signal detection. The asymptotic properties help quantify these effects and thus provide guidance in choosing an appropriate threshold.

The relationship between H-volatility and market volatility further informs practical aspects of trading, such as setting stop-loss levels and determining position sizes. Specifically, since the average significant price movement converges to $2\sigma H$, stop-loss orders can be placed at distances proportional to H, ensuring that risk limits are aligned with the expected variability of the price process. This approach helps strike a balance between avoiding excessive sensitivity to normal fluctuations and maintaining sufficient exposure to capture meaningful trends.

The asymptotic regularity of H-inversion and H-volatility under specific stochastic models facilitates the integration of Renko and Kagi charts into algorithmic trading frameworks. Algorithms can be designed to trigger trading signals when an H-inversion is detected or when predefined H-volatility thresholds are crossed. By automating the identification of significant price movements, such systems enable faster adaptation to market conditions and help mitigate the influence of behavioral biases.

Although the Wiener process provides a foundational benchmark for analyzing these constructions, real financial markets display features that go beyond simple Brownian motion. These include discontinuous jumps, heavy-tailed return distributions, volatility clustering, and long-memory effects. Extending the analysis to alternative stochastic processes allows for a more realistic representation of market dynamics and enhances the practical relevance of Renko and Kagi-based methods.

Incorporating jumps into the price process, as modeled by Lévy processes, fundamentally alters both the frequency and magnitude of significant price movements. Jumps create discontinuities that can trigger multiple effective reversals in a single event, thereby reshaping the statistical properties of H-inversion and H-volatility. Studying Renko and Kagi constructions

under Lévy dynamics thus provides valuable insights into markets subject to sudden shocks, such as those driven by macroeconomic news or liquidity shortages.

Stochastic volatility models, such as the Heston model, capture the empirically observed phenomenon of volatility clustering. In this framework, the volatility parameter $\sigma_{(t)}$ evolves as a stochastic process, making the distributional properties of H-volatility and H-inversion explicitly time- and state-dependent. This setting offers a richer ground for analyzing risk dynamics and improving option pricing as well as volatility forecasting.

Finally, fractional Brownian motion (fBM) incorporates long-range dependence via the Hurst exponent $H \in (0,1)$. When $H > 0.5$, the process exhibits persistence, leading to fewer trend reversals and more extended trends; when $H < 0.5$, it exhibits anti-persistence, generating more frequent reversals consistent with mean-reverting dynamics. Since fBM lacks the independent increments property of standard Brownian motion, the asymptotic behavior of H-inversion and H-volatility deviates systematically from the Wiener benchmark. This provides a natural framework for modeling markets with memory effects, such as emerging markets or assets with strong institutional trading patterns.

2.4 Trading Strategies Based on Renko and Kagi Constructions

The Renko and Kagi constructions not only serve as powerful tools for visualizing significant price movements but also provide a robust foundation for systematic trading strategies. By exploiting the statistical properties of H-constructions introduced in the previous sections, one can formulate rules that align with the underlying dynamics of the price process. Broadly, two classes of strategies emerge: momentum (trend-following) strategies and contrarian (mean-reversion) strategies. Although the empirical implementation in this study focuses on the contrarian approach—owing to its compatibility with mean-reverting spread processes—we briefly outline the momentum strategy for conceptual completeness.

An H-strategy refers to a trading rule directly linked to the H-construction of either Renko or Kagi charts, where the threshold H defines the minimal significant price movement. These strategies are formulated using the sequences of stopping times $\{s_n^a\}$ and $\{s_n^b\}$, as defined in Sections 2.1 and 2.2, representing local extrema and confirmation points of reversals,

respectively. Since the distinction between Renko and Kagi constructions is minor for trading implementation, we treat them jointly under the umbrella of H-strategies.

The momentum strategy seeks to exploit the continuation of established trends. A trader enters a long position at time s_n^b when the price process confirms a breakout above the previous local maximum $P(s_{n-1}^a)$, and conversely enters a short position when the price breaks below the previous local minimum. The corresponding trading signals are:

Buy if $P(s_n^b) - P(s_n^a) > 0$ or $P(s_n^a) - P(s_{n-1}^a) > 0$ (upward breakout);

Sell if $P(s_n^b) - P(s_n^a) < 0$ or $P(s_n^a) - P(s_{n-1}^a) < 0$ (downward breakout).

The profit from a single trade executed between the stopping times s_{n-1}^b and s_n^b is given by:

$$Y_{s_n^b} = (P(s_n^b) - P(s_{n-1}^b)) \cdot sign\ (P(s_n^a) - P(s_{n-1}^a)) \tag{22}$$

Aggregating over the interval [0, T], the total profit can be expressed (up to a first-order approximation) as:

$$Y_T(H,P) \approx (v_T(H,P) - 2H) \cdot N_T(H,P) \tag{23}$$

where $v_T(H,P)$ is the H-volatility and $N_T(H,P)$ is the H-inversion, as defined in Section 2.3. Equation (23) reflects the intuition that each effective price reversal contributes an average payoff equal to the excess movement $v_T(H,P) - 2H$, multiplied by the total number of reversals.

The contrarian strategy builds on the premise that prices tend to revert to their mean after substantial movements. Within the H-construction framework, a trader following this approach would short the asset at a stopping time s_n^b after a significant upward move, anticipating a subsequent decline, and go long at s_n^b after a significant downward move, expecting a rebound. The trading rules can be summarized as:

Sell if $P(s_n^b) - P(s_n^a) > 0$ or $P(s_{n-1}^a) - P(s_n^a) > 0$;

Buy if $P(s_n^b) - P(s_n^a) < 0$ or $P(s_{n-1}^a) - P(s_n^a) < 0$.

The profit from a single trade executed between s_{n-1}^b and s_n^b is defined as:

$$Y_{s_n^b} = (P(s_n^b) - P(s_{n-1}^b)) \cdot sign\ (P(s_{n-1}^a) - P(s_n^a)) \tag{24}$$

Aggregating over the interval [0, T], the cumulative profit can be approximated as:

$$Y_T(H,P) \approx (2H - v_T(H,P)) \cdot N_T(H,P) \tag{25}$$

where $v_T(H,P)$ denotes the H-volatility and $N_T(H,P)$ the H-inversion.

Comparing equations (23) and (25), it is clear that the profitability of H-strategies critically depends on the relationship between $v_T(H,P)$ and $2H$. Specifically:

- If $v_T(H,P) > 2H$, momentum strategies yield positive profits, while contrarian strategies incur losses;
- If $v_T(H,P) < 2H$, contrarian strategies become profitable, while momentum strategies lose money;
- If $v_T(H,P) = 2H$, both strategies break even, producing zero expected profit.

As established in Section 2.3, for processes like the standard Wiener process, the H-volatility converges to $v_T(H,W) = 2H$ as $T \to \infty$. This implies that neither the momentum nor the contrarian strategy would generate profit when applied to a pure Brownian motion, consistent with the efficient market hypothesis.

More generally, the profitability of H-strategies is closely linked to the statistical properties of the underlying price process. For martingale processes with independent and identically distributed increments and zero drift (e.g., the Wiener process), we have $v_T(H,P) = 2H$, leading to zero expected profit for both strategies. For mean-reverting processes, such as the OU process, the H-volatility $v_T(H,P)$ is typically less than $2H$. In this case, contrarian strategies become potentially profitable, as prices are more likely to revert after significant deviations. Conversely, if the price process has a drift or exhibits persistent trends, then $v_T(H,P)$ may exceed $2H$, favoring momentum strategies.

In practical financial markets, asset prices rarely behave as perfect martingales. Mean-reversion is often observed in certain asset classes such as currencies, commodities, and correlated stock pairs, where contrarian strategies can be effective. Conversely, strong trending markets may provide profitable opportunities for momentum strategies.

When implementing H-strategies based on Renko and Kagi constructions, several practical considerations arise. Transaction costs—such as trading fees, bid–ask spreads, and slippage—can materially reduce profitability, especially for high-frequency strategies. Short-selling restrictions may further limit the feasibility of taking both long and short positions. Moreover, the effectiveness of momentum versus contrarian strategies is often regime-dependent: periods of

elevated volatility or structural changes in the market may alter the statistical properties of $P(t)$, thereby shifting the balance between the two approaches. Finally, selecting an appropriate threshold H is critical. A small H increases sensitivity to price movements but amplifies noise, while a large H filters noise but may delay signals. Robust backtesting and empirical calibration are therefore essential for optimizing strategy performance.

3. Extended Properties of Renko and Kagi Constructions

3.1 Properties of H-Constructions on the Ornstein–Uhlenbeck Process

The OU process is a fundamental stochastic process widely used to model mean-reverting behavior in financial time series. It is defined by the stochastic differential equation (SDE):

$$dX_t = -\theta(X_t - \mu)dt + \sigma dB_t \tag{26}$$

where $\theta > 0$ is the rate of mean reversion, μ is the long-term mean level, $\sigma > 0$ is the volatility parameter, and B_t is a standard Brownian motion. For analytical convenience, and without loss of generality, we may set $\mu = 0$, yielding the simplified SDE:

$$dX_t = -\theta X_t dt + \sigma dB_t \tag{27}$$

The OU process exhibits a natural tendency to revert to its mean level, which makes it a suitable model for assets or spreads displaying mean-reverting characteristics. When applying H-constructions (Renko or Kagi charts) to the OU process, it is important to understand how their properties differ from those observed with non-mean-reverting processes such as the standard Wiener process discussed in Section 2.3.

In the framework of H-constructions, the H-volatility $v_T(H, P)$ plays a critical role in determining the profitability of trading strategies. Recall that for the Wiener process, $v_T(H, W) \to 2H$ as $T \to \infty$, leading to zero expected profit for both momentum and contrarian strategies. By contrast, the mean-reverting nature of the OU process affects the H-volatility significantly: large deviations are less likely to persist, and the process is more likely to reverse direction before reaching a magnitude of H.

A key asymptotic property of the OU process is that its H-volatility satisfies $H \leq v_T(H, P) < 2H$ for $T \to \infty$. This inequality reflects the fact that the H-volatility for the OU

process is strictly less than $2H$, but typically bounded away from zero and close to or above H, owing to the mean-reverting structure of the process.

Theorem 3.1. Let $P(t)$ follow the OU process defined in (26), and let $v_T(H, P)$ denote the H-volatility under a Renko or Kagi construction. Then, as $T \to \infty$,

$$\lim_{T \to \infty} v_T(H, P) < 2H \tag{28}$$

The mean-reverting nature of the OU process causes price movements to reverse more frequently and with smaller magnitudes compared to a pure random walk. As a consequence, the average significant price movement per trend reversal (captured by the H-volatility) is strictly less than the benchmark value $2H$ obtained for the Wiener process.

Given that $v_T(H, P) < 2H$ for the OU process, contrarian (mean-reversion) H-strategies become theoretically profitable. According to the profit formula:

$$Y_T(H, P) = (2H - v_T(H, P)) \cdot N_T(H, P) \tag{29}$$

where $Y_T(H, P)$ is the total profit over the period [0, T] and $N_T(H, P)$ is the H-inversion, representing the number of significant price reversals. Since $(2H - v_T(H, P)) > 0$ for the OU process, the expected total profit $Y_T(H, P)$ is positive under the assumptions of zero transaction costs and unrestricted trading. A detailed proof is provided in Appendix A.

Assets or spreads modeled by an OU process are natural candidates for contrarian strategies. Examples include interest rate spreads, currency pairs with pegged exchange rates, and certain commodity spreads. The choice of the threshold H is crucial: a smaller H captures more frequent reversals but may be overly sensitive to noise, while a larger H produces clearer signals at the cost of fewer opportunities. In practice, transaction costs, bid–ask spreads, and slippage can significantly erode the theoretical profitability.

The theoretical results also rely on the assumption that the OU process parameters θ and σ remain constant. In real markets, these parameters are time-varying, requiring ongoing calibration. Numerical simulations and empirical studies confirm that $v_T(H, P)$ converges to a value strictly below $2H$. This reinforces the potential profitability of contrarian strategies in mean-reverting markets when implemented with Renko and Kagi constructions.

3.2 Properties of H-Constructions on the Discrete Process

In practical applications, financial data are typically recorded at discrete time intervals (e.g., daily closing prices), rather than continuously. This discreteness introduces certain challenges when applying H-construction methods, such as Renko or Kagi charts, which were originally designed for continuous processes. In this section, we explore the properties and implications of applying H-constructions to discrete stochastic processes, focusing on the random walk and the autoregressive AR(1) process.

3.2.1 Random Walk

Consider a discrete-time stochastic process $\{Y(t)\}$ defined as the cumulative sum of independent and identically distributed (i.i.d.) random variables:

$$Y(t) = \sum_{i=0}^{t} X(i), \ \ X(i) \sim N(0, \sigma^2), t = 0,1,2, \dots \tag{30}$$

This process $\{Y(t)\}$ is a simple Gaussian random walk. When attempting to apply the H-construction to $\{Y(t)\}$, we encounter an issue stemming from the discrete sampling of the process. Specifically, the probability that the process moves exactly H units between two discrete observation times is zero:

$$P(|Y(t + n) - Y(t)| = H) = 0, \ \forall n \geq 1, t \geq 0 \tag{31}$$

In continuous time (e.g., for Brownian motion), threshold crossings occur exactly at level H. However, in discrete time, because we only observe the process at sampled points, crossings typically occur with an overshoot, i.e., the process jumps beyond H rather than hitting it precisely.

Formally, at each stopping time s_{b_n} where the process crosses the threshold H, we observe an overshoot $\widetilde{H}_n$ such that:

$$|Y(s_{a_n}) - Y(s_{b_n})| = \widetilde{H}_n \geq H \tag{32}$$

where $\widetilde{H}_n$ is a random variable representing the actual movement, which is at least H but possibly larger due to the continuous increments being sampled only at discrete times.

This overshoot leads to an upward bias in the empirical H-volatility relative to the idealized continuous-time case. In particular, the expected number of H-inversions over a time horizon T, denoted $n_T(H, Y)$, satisfies:

$$n_T(H,Y) = \frac{2E[\widetilde{H}_n]}{H} \geq 2 \text{ or } v_T(H,Y) = 2E[\widetilde{H}_n] \geq 2H$$

where the benchmark value of 2 corresponds to the continuous-time martingale case. Thus, overshoots inflate the measured H-volatility, even though the underlying process remains a martingale.

In practical terms, when applying H-constructions to real-world discrete financial data, one often observes an H-volatility greater than the theoretical benchmark of 2. Importantly, this does not imply non-martingale behavior, nor does it suggest that a trend-following H-strategy would be profitable. The inflation is simply a consequence of overshoot effects, which are especially pronounced when the increment standard deviation σ is comparable in magnitude to the threshold H.

To better understand the overshoot, we examine its dependence on the ratio H/σ. When H is large relative to σ, the expected overshoot is small and $E[\widetilde{H}_n] \rightarrow H$. Conversely, when H is small relative to σ, the overshoot becomes larger on average, leading to a greater upward bias in the empirical H-volatility $v_T(H,Y)$.

3.2.2 Autoregressive Process $AR(1)$

Next, we examine the first-order autoregressive process, AR(1), which can be regarded as a discrete-time analogue of the OU process:

$$Y(t) = \alpha Y(t-1) + X(t), \; X(t) \sim N(0,\sigma^2), \; t = 1,2,\ldots \tag{33}$$

where, $\alpha \in [0,1)$ is the autoregressive coefficient that determines the degree of mean reversion. When $|\alpha| < 1$, the process is stationary with variance $Var(Y) = \sigma^2/1 - \sigma^2$.

As in the random walk case, the AR(1) process does not satisfy the conditions required for precise H-construction steps, since the increments have a continuous distribution:

$$P(|Y(t+n) - Y(t)| = H) = 0, \; \forall n \geq 1, \; t \geq 0 \tag{34}$$

Thus, crossings of the threshold H occur with an overshoot at each stopping time s_{b_n}:

$$|Y(s_{a_n}) - Y(s_{b_n})| = \widetilde{H}_n \geq H \tag{35}$$

where $\widetilde{H}_n$ is a random variable representing the actual displacement.

A key difference from the random walk is that the AR(1) process exhibits mean-reverting behavior. Although it is not strictly bounded, its stationary distribution has finite variance, which effectively restricts the typical range of fluctuations. This feature implies that overshoots are less extreme compared to the random walk, where variance grows without bound.

Regarding overshoot behavior, while the expected overshoot $E[\widetilde{H}_n]$ decreases as H increases, it generally remains strictly larger than H. Unlike the random walk case, where $E[\widetilde{H}_n] \to H$ when $H \gg \sigma$, the mean-reverting structure of the AR(1) process prevents the overshoot from converging precisely to H.

Consequently, it is possible to observe an H-volatility measure exceeding the theoretical benchmark of 2, $n_T(H,Y) \geq 2$, without contradicting Theorem 3.1. This behavior is consistent with the properties of discrete mean-reverting processes and reflects the presence of overshoot rather than a violation of martingale conditions.

To quantify this effect, we define the expected overshoot empirically as:

$$E[\widetilde{H}_n] = \frac{1}{N}\sum_{n=1}^{N} |Y(s_{a_n}) - Y(s_{b_n})| \tag{36}$$

and introduce the ratio,

$$R(H,Y) = \frac{n_T(H,Y)}{2E[\widetilde{H}_n]} \in [1,\infty) \tag{37}$$

This ratio measures the deviation of the observed H-volatility from the continuous-time benchmark, providing a convenient way to quantify the inflation due to overshoot in the AR(1) process.

3.2.3 Implications for Trading Strategies and Parameter Selection

When implementing H-strategies on discrete processes, the overshoot phenomenon introduces several practical considerations that directly affect trading performance.

First, overshoots influence trading profitability. In contrarian strategies, overshoots can be beneficial: since the strategy takes positions opposite to recent price movements, trades are entered at more favorable levels—higher for short positions and lower for long positions. This mechanism may improve profitability compared to the continuous-time benchmark. Conversely, in trend-following strategies, overshoots tend to reduce profitability, as trades are executed only

after the price has already moved beyond the threshold H, resulting in less advantageous entry points.

Second, overshoots impact transaction costs. Because the realized displacement $\widetilde{H}_n$ is larger than H, the effective gain per trade can deviate from the theoretical expectation. A useful proxy for evaluating the cost-to-gain balance is the ratio $k/E[\widetilde{H}_n]$, where k denotes transaction costs. A higher ratio indicates that transaction costs consume a larger fraction of expected per-trade gains, potentially eroding overall profitability, particularly when H is small relative to σ.

Selecting appropriate values for the threshold H and time horizon T is therefore crucial for the success of H-strategies on discrete processes. There is a fundamental trade-off between overshoot effects and trading frequency. Increasing H reduces the relative magnitude of overshoots, since $E[\widetilde{H}_n] \to H$ as $H/\sigma \to \infty$. This improvement enhances the ratio $R(H,Y)$ and lowers the proportion of costs relative to gains. However, decreasing H increases the number of H-inversions $n_T(H,Y)$, leading to more trading opportunities and potentially higher aggregate profits. At the same time, overshoot effects become more pronounced and transaction costs represent a larger share of profits.

Thus, there exists an optimal value of H that maximizes profitability by balancing the trade-off between trade frequency, overshoot effects, and transaction costs. This optimal threshold depends on the properties of the underlying process $Y(t)$, including its volatility σ, the degree of autocorrelation α (in AR(1) processes), and the level of transaction costs k. In addition, ensuring statistical reliability requires a sufficient number of H-inversions $n_T(H,Y)$. This condition may necessitate either extending the observation horizon T or selecting a smaller H to increase the number of data points.

Further refinements can be achieved through adaptive strategies, in which H is allowed to vary with market conditions. For example, the threshold can be scaled with volatility forecasts (e.g., from a GARCH model), thereby maintaining a roughly constant ratio between H and σ and mitigating the overshoot effect. Moreover, analyzing the empirical distribution of overshoots $\widetilde{H}_n$ provides valuable insights. In particular, trades associated with unusually large overshoots, such as $\widetilde{H}_n > 2H$, may lead to adverse outcomes in contrarian strategies, as subsequent mean

reversion may be insufficient to generate profits. Filtering or adjusting strategies around such scenarios can further improve performance.

In summary, applying H-constructions to discrete financial processes introduces complexities absent in continuous models. Overshoots not only bias the measurement of H-volatility but also affect the profitability and robustness of trading strategies. Careful selection of the threshold H, together with an understanding of the underlying process characteristics, is essential for optimizing trading performance. Adaptive thresholds and overshoot-aware adjustments offer promising avenues for enhancing the effectiveness of H-strategies in practical financial applications.

4. Pairs Trading Based on the Contrarian H-strategy

Pairs trading strategies typically consist of three steps: (i) the formation of pairs, (ii) the rule for opening a position on the spread, and (iii) the rule for closing the position. In the contrarian H-strategy, however, the latter two steps are unified into a single reversal rule: the signal to close an existing position simultaneously serves as the signal to open a new position in the opposite direction. This section outlines the construction of the strategy based on Kagi charts, together with the dataset and testing methodology employed in the empirical analysis.

4.1 Data

To evaluate the effectiveness of contrarian H-strategies in pairs trading, we employ daily adjusted closing prices of stocks from both the U.S. and Chinese markets. The Chinese stock market data are obtained from the iFinD database, while the U.S. data are cross-checked with publicly available datasets to ensure consistency. The study covers several major indices of varying capitalization levels. For each index, we adopt the rolling constituent approach, meaning that the sample includes the constituent stocks corresponding to each year of the testing period.

Table 1 summarizes the datasets used, including the number of constituents, the full sample period, and the designated out-of-sample testing window. The out-of-sample period begins one year after the start of the full sample period, reflecting the standard one-year formation and one-year trading structure of Gatev et al. (2006). This cross-market setting allows us to examine the

robustness of the contrarian H-strategy across different institutional environments and capitalization structures, providing a comprehensive basis for comparison.

Table 1. Dataset Overview: Constituents and Sample Periods.

Stock indexes	Number of constituents	Entire data period	Out-of-sample period
S&P 500	500	Jan 1995-June 2024	Jan 1996-June 2024
CSI 300	300	Jan 2005-June 2024	Jan 2006-June 2024
CSI 100	100	Jan 2006-June 2024	Jan 2007-June 2024
CSI 200	200	Jan 2007-June 2024	Jan 2008-June 2024
CSI 500	500	Jan 2007-June 2024	Jan 2008-June 2024

Note: For the Number of constituents, this paper includes the constituent stocks for each year.

- **S&P 500 Index**: The S&P 500 comprises 500 leading large-cap U.S. companies across a broad range of sectors. The dataset spans from January 1995 to June 2024, offering nearly three decades of historical data for robust empirical analysis. The testing period begins in January 1996 and extends to June 2024 under a rolling formation-and-trading framework. This dataset enables us to evaluate the performance of pairs trading strategies in a relatively mature and efficient market.

- **CSI 300 Index**: The CSI 300 consists of 300 of the largest and most liquid A-share stocks listed on the Shanghai and Shenzhen stock exchanges. The dataset covers the period from January 2005 to June 2024, with the testing period starting in January 2006 and continuing until June 2024 under the rolling framework. As the primary benchmark for the Chinese equity market, this dataset allows us to examine the behavior of pairs trading strategies in an emerging market setting.

- **CSI 100 Index**: The CSI 100 represents the top 100 companies by market capitalization within the CSI 300, the CSI 100 dataset spans from January 2006 to June 2024, with the testing period beginning in January 2007. By focusing on the largest Chinese firms, this dataset facilitates the assessment of pairs trading strategies among the most prominent and potentially more efficient segment of the Chinese market.

- **CSI 200 Index**: The CSI 200 comprises the next 200 largest firms following the CSI 100, representing mid-cap stocks. The data cover the period from January 2007 to June 2024, with the testing period starting in January 2008. This dataset enables the analysis

of pairs trading strategies in the mid-cap segment, which may display distinct market dynamics relative to large-cap firms.

- **CSI 500 Index**: The CSI 500 consists of 500 small-cap companies and spans the period from January 2007 to June 2024, with the testing period beginning in January 2008. By incorporating small-cap firms, this dataset provides an opportunity to examine pairs trading strategies in a segment that is potentially less efficient and more volatile compared to large- and mid-cap stocks.

Each dataset contains the constituent stocks for each year within the sample period, ensuring that changes in index composition are properly incorporated into the analysis. Pairs trading strategies aim to exploit temporary mispricings between correlated securities, thereby capitalizing on market inefficiencies. The profitability of such strategies is expected to vary with the degree of market efficiency across different indexes. In general, large-cap stocks, such as those in the S&P 500 and CSI 100, tend to operate in relatively efficient markets due to higher liquidity and greater analyst coverage. In contrast, mid-cap and small-cap stocks, represented by the CSI 200 and CSI 500, may exhibit lower levels of efficiency, thereby offering greater opportunities for profitable pairs trading.

Accordingly, we hypothesize that pairs trading strategies will yield higher returns in the CSI 500, where market inefficiencies are more pronounced, compared with the larger and more efficient stocks in the CSI 100. Examining the profitability of pairs trading across market segments thus provides an indirect measure of relative market efficiency, since higher abnormal returns are typically indicative of lower efficiency.

Following Gatev et al. (2006), we adopt a formation–trading period framework. Specifically, a 12-month formation period is used to identify potential pairs and calibrate the trading model, followed by a 6-month trading period in which these pairs are actively traded. The trading commences on the first business day after the formation period and continues until the end of the designated horizon. For example, in the case of the S&P 500 dataset, the first formation window spans January 1995 to December 1995, with the corresponding trading window from January 1996 to June 1996. This framework is consistently applied across all datasets, with adjustments to the start date according to data availability (see Table 1).

To enhance robustness, we generate overlapping trading periods. Each month, a new formation period concludes and a new trading period begins, resulting in multiple concurrent trading windows for most months. Returns are then averaged across overlapping periods to obtain more stable estimates.

Notably, our sample includes periods of heightened volatility, such as the Global Financial Crisis (GFC), the Bull and Bear (BNB) cycle, and the COVID-19 pandemic. Although short-selling restrictions were temporarily imposed during the GFC, the pairs trading strategy remains applicable, as institutional investors managing diversified portfolios can implement the trades through intra-portfolio adjustments rather than traditional short-selling mechanisms.

4.2 Stocks Pre-Selection

To evaluate our pairs trading strategy, we carefully selected stocks from multiple datasets, emphasizing liquidity and market representativeness. For the S&P 500 and CSI 300 indexes, which consist of large-cap and highly liquid stocks, we employed the entire set of constituents without applying additional liquidity filters. These indexes inherently include well-traded, high–market-cap companies, ensuring that our strategy is tested on stable and widely traded assets. Larger companies generally exhibit lower levels of mispricing because they attract significant attention from institutional and individual investors. Consequently, we expect the profit estimates from these datasets to be relatively conservative.

For the CSI 100 and CSI 200 indexes, which represent large-cap and mid-cap subsets of the CSI 300, we also included all constituents without further filtering. This design allows us to assess the performance of the strategy across different tiers of market capitalization within the Chinese market and to evaluate how market efficiency and liquidity affect profitability in large-cap versus mid-cap segments.

To explore the potential for higher returns in less efficient markets, we incorporated the CSI 500 index, which comprises small-cap companies. These stocks are more prone to mispricing due to limited analyst coverage and lower investor attention, but they also pose greater liquidity challenges. To mitigate this issue, we applied a liquidity filter based on trading activity. Specifically, we required that each stock have no more than ten non-trading days during the 12-month formation period used for strategy calibration. This threshold, less strict than

requiring uninterrupted trading, accounts for occasional suspensions due to corporate announcements or regulatory interventions. By allowing up to ten such days, we expand the stock pool while preserving the dataset's reliability for pairs trading.

During the trading period, if a stock experienced a non-trading day—indicated by zero price or volume—we carried forward its previous day's closing price to maintain continuity in spread calculations. However, no positions were opened or closed on those days, regardless of any trading signals generated, since transactions cannot be executed when the stock is inactive. This rule aligns the backtest with realistic market conditions.

Consistent with industry practice, we used opening and closing auction prices for trade entries and exits to reduce the impact of bid–ask spread variations. In both the U.S. and Chinese markets, these prices reflect high trading volumes and can be executed with greater confidence.

Finally, we imposed no additional filters such as sector or industry classifications. This open selection framework ensures that the strategy adapts dynamically to diverse market conditions and provides a comprehensive assessment of each dataset's potential for pairs trading opportunities.

4.3 Pairs Formation Criteria

We take the logarithm of the prices of all stocks pre-selected for pairs trading based on the 12-month historical period (January 2004 to December 2004). For each dataset—All stocks, CSI 100, CSI 200, and CSI 500—we construct all possible stock pairs and define their spread process as:

$$y_{i,j}(t) = logP_i(t) - logP_j(t) \tag{38}$$

where $P_i(t)$ and $P_j(t)$ are the prices of stocks i and j on day t.

For each spread process, we compute its standard deviation $\sigma_{i,j}$. The threshold parameter $H_{i,j}$ in the H-strategy is set equal to this standard deviation:

$$H_{i,j} = \sigma_{i,j}$$

Next, we apply the H-construction to each spread and calculate two key measures: the H-volatility $v_{i,j}(H_{i,j})$ and H-inversion $N_{i,j}(H_{i,j})$. All pairs are then ranked in descending

order by their H-inversion. Pairs with higher H-inversion values are expected to exhibit stronger mean-reversion behavior during the trading period and therefore provide greater profit opportunities.

The H-inversion captures several important aspects of the spread. First, a smaller spread standard deviation (analogous to the squared distance in Gatev et al., 2006) implies a smaller H, which generally leads to a higher H-inversion. Second, for two spreads with the same H and $v(H)$, a larger H-inversion indicates higher potential profitability, as established in Section 3.2.3. Finally, a larger H-inversion corresponds to a larger sample size in the H-construction, which enhances the statistical reliability of the calibration.

For each dataset, we select the top N pairs with the highest H-inversion values. Unlike some earlier studies, we restrict each stock to appear in only one selected pair. This one-to-one matching rule avoids situations where the same stock could be traded long in one pair and short in another simultaneously. Although this restriction may exclude some profitable combinations, it enhances portfolio diversification and prevents overlapping exposures.

4.4 Trading Rules

Trading begins on the first day of the trading period for all pairs selected during the formation stage and continues until the final day, at which point all open positions are closed. This design ensures continuous market exposure, allowing us to capture profit opportunities as they arise.

To determine the initial trading direction for each pair, we apply the H-construction to the historical formation period using the calibrated parameter $H_{i,j}$ (see Section 4.3). We then examine the spread process $y_{i,j}(t) = log P_i(t) - log P_j(t)$ at the end of the formation period to identify its last local extremum. This step ensures that the virtual trading during the formation period transitions seamlessly into real trading in the subsequent six-month trading period.

If the spread ends with a local maximum, we open a long spread position on the first day of trading by buying stock i and selling short stock j. This setup reflects the expectation that the spread will mean-revert downward from its local maximum toward a local minimum. Conversely,

if the spread ends with a local minimum, we open a short spread position (sell stock i, buy stock j), anticipating that the spread will revert upward toward a local maximum.

We monitor the spread process $y_{i,j}(t)$ and generate trading signals using the H-construction. A sell signal occurs at the first time t after the last stopping time s_{b_0} of the formation period such that:

$$y_{i,j}(t) - \min_{s_{b_0} \leq n \leq t} y_{i,j}(n) \geq H_{i,j} \tag{39}$$

This condition identifies the moment when the spread has moved upward by more than $H_{i,j}$ from its most recent local minimum, thereby recognizing the occurrence of a new local minimum. Upon receiving the sell signal at $s_{b_1} = t$, we reverse our position from long to short. Specifically, we close the existing long position by selling stock i and buying back stock j, and simultaneously open a new short position on the spread by shorting stock i and going long in stock j.

We continue to track the spread process $y_{i,j}(t)$ until the next buy signal, which occurs at the first time t after s_{b_1} such that:

$$\max_{s_{b_1} \leq n \leq t} y_{i,j}(n) - y_{i,j}(t) \geq H_{i,j} \tag{40}$$

This condition indicates that the spread has declined by more than $H_{i,j}$ from its most recent local maximum, thereby identifying a new local maximum. At this point, we reverse our position back to long on the spread.

The procedure is applied iteratively throughout the trading horizon. The strategy remains continuously invested, alternating between long and short positions in the spread according to the signals generated by the H-construction. On the last day of the trading period, all open positions are liquidated to conclude the trading cycle.

If the spread process ends at a local minimum at the conclusion of the formation period, we adjust our initial trading action accordingly. In this case, we establish a short position in the spread by shorting stock i and buying stock j, anticipating that the spread will increase from this local minimum toward the next local maximum. Thereafter, the same H-construction rules are applied as described above.

We apply the H-construction trading strategy consistently across all four datasets. In the All Stocks sample, the method effectively identifies and exploits spread relationships even within a highly diverse stock universe. The large number of available pairs generates ample trading opportunities, though liquidity constraints in smaller-cap stocks warrant caution. For the CSI 100 dataset, the high liquidity and market prominence of these large-cap constituents facilitate trade execution at desired prices. The relatively stable comovements among blue-chip stocks further support consistent strategy performance. In contrast, trading within the CSI 200 and CSI 500 universes involves mid- and small-cap stocks, where higher volatility and liquidity frictions may arise. Nevertheless, the H-construction remains applicable, with appropriate adjustments made to reflect the specific characteristics of these market segments.

By adhering to the defined trading rules and systematically applying the H-strategy, we seek to generate robust profitability across varying market conditions and datasets. Continuous market engagement and disciplined position management constitute key features of the strategy, enabling us to capitalize on the mean-reverting dynamics of spread processes identified during the formation period.

4.5 Excess Returns and Transaction Costs

To evaluate the excess returns of our pairs trading strategy, we follow the methodology commonly used in the literature (e.g., Gatev et al., 2006; Do and Faff, 2010). The strategy maintains a dollar-neutral position by investing \$1 in both the long and short legs of each pair. Value-weighted daily mark-to-market cash flows from each pair are computed and interpreted as excess returns.

The daily excess return of the portfolio, $r_{P,t}$, is calculated using the formula:

$$r_{P,t} = \frac{\sum_{i \in P} w_{i,t}\, c_{i,t}}{\sum_{i \in P} w_{i,t}} \tag{41}$$

where, $c_{i,t}$ is the daily cash flow from pair i. $w_{i,t}$ represents the weight of pair i at time t.

At initiation, each pair is assigned a unit weight ($w_{i,0} = 1$), which evolves over time as:

$$w_{i,t} = w_{i,t-1}\,(1 + c_{i,t-1}) = \prod_{s=1}^{t-1}(1 + c_{i,s}) \tag{42}$$

The daily cash flow or return from a pair is given by:

$$c_i(t) = \sum_{j=1}^{2} I_j(t) v_j(t) r_j(t) \tag{43}$$

where $I_j(t)$ is an indicator variable, equal to 1 if a long position is held in stock j at time t, and -1 if a short position is held. $r_j(t)$ is the daily return of stock j. $v_j(t)$ is the weight of stock j, used to calculate daily cash flows, and evolves as:

$$v_j(t) = v_{j,t-1}(1 + r_{j,t-1}) = \prod_{s=1}^{t-1}(1 + r_j(s)) \tag{44}$$

Daily excess returns are then compounded to obtain monthly returns.

Transaction costs are known to significantly affect the profitability of pairs trading. Bowen et al. (2010) reported a reduction of more than 50% in excess returns for high-frequency strategies when a fee of 15 basis points was applied. Similarly, Do and Faff (2012), in replicating Gatev et al. (2006), found that incorporating realistic transaction costs rendered the strategy unprofitable.

In our baseline analysis, we assume transaction costs of 0.30% (30 bps) per trade, reflecting average retail brokerage fees in the Chinese market as of June 2024. For comparison, U.S. brokerage fees are generally lower, with commissions often below 0.10% per trade, particularly for stocks priced above $5. Accordingly, a 0.10% cost per trade translates into an effective round-trip cost of approximately 0.20% per stock, or 0.40% for the pair as a whole.

To incorporate transaction costs into our calculations, we adjust the cash flows when the direction of the trade changes at stopping times s_{bn}. Specifically, we reduce the current day's cash flow by the weighted transaction costs:

$$c_i(s_{bn}) = \sum_{j=1}^{2}\left[I_{j,t} v_{j,t}\, r_{j,t} - k\, v_{j,t}(1 + r_{j,t})\right], s_{bn} = t \tag{45}$$

where $k = 0.0010$ denotes the fee rate per transaction. Additionally, when new positions are established on the next trading day, the total round-trip cost of $2 is reflected by deducting 2k from the cash flow:

$$c_i(s_{b_{n+1}}) = c_i(s_{b_{n+1}}) - 2k \tag{46}$$

While our assumed transaction costs are conservative for institutional settings, they provide a realistic benchmark for retail investors. We report strategy performance both before and after transaction costs. Readers may scale our estimates by applying their preferred per-trade

cost to the effective round-trip trading volume (approximately $2 per pair) and multiplying by the average trade frequency reported in the results section.

Finally, it is important to note that pairs trading inherently employs leverage. Since the strategy invests $1 in each leg, the effective leverage ratio is 2:1, while excess returns are computed relative to $1 of notional capital. Brokerage fees are thus applied on the full $2 trading volume, which must be considered when comparing our results with those from non-leveraged benchmarks such as passive buy-and-hold strategies.

5. Results

5.1 Profitability of the Strategies

Table 2 provides a comprehensive analysis of the monthly excess returns generated by the Kagi and Renko pairs trading strategies across various market indices. The table is divided into two panels: Panel A focuses on Kagi constructions, while Panel B examines Renko constructions. This analysis evaluates the performance, statistical significance, and characteristics of both strategies across different market environments.

Both strategies generate positive mean monthly excess returns across all indices, as shown in Figure 4. For the Kagi strategy, the mean returns range from 0.0047 (CSI 100) to 0.0093 (S&P 500). The t-statistics for all indices are significant at the 99% confidence level, indicating that the excess returns are statistically different from zero. Similarly, for the Renko strategy, mean returns vary from 0.0053 (CSI 100) to 0.0089 (S&P 500), with all t-statistics also significant at the 99% confidence level. These findings suggest that both strategies generate robust and consistent profits, particularly in the S&P 500, which shows higher mean returns compared to the CSI indices.

Comparing the two strategies, Kagi generally exhibits slightly higher mean returns than Renko in the S&P 500 and CSI 300, whereas Renko is marginally higher in CSI 100, CSI 200, and CSI 500. Volatility levels are similar, with monthly standard deviations tightly clustered around 0.014–0.017 across indices; consequently, cross-method Sharpe differences are driven primarily by mean-return gaps, with volatility playing a secondary role. For example, in CSI 500 the mean-only approximation nearly reproduces the observed Sharpe gap (predicted −0.078 vs. actual −0.079), while in the S&P 500 and CSI 300 modestly higher volatility for Renko further

widens Kagi's Sharpe advantage. Sharpe ratios therefore still differentiate performance: Kagi outperforms in the S&P 500 and CSI 300, whereas Renko achieves higher Sharpe ratios in CSI 100, CSI 200, and CSI 500. Notably, Renko's best absolute Sharpe still occurs in the S&P 500 (0.6079), and in absolute terms both methods attain their highest risk-adjusted performance in the S&P 500. This pattern is consistent with Kagi capturing shorter-horizon reversals more effectively in efficient venues, while Renko remains relatively competitive across several CSI segments.

The distribution characteristics further distinguish the two strategies. For the Kagi strategy, skewness values vary across indices, with positive skewness observed in the S&P 500 and CSI 300, indicating a longer right tail (more extreme positive returns), and negative skewness in the CSI 100 and CSI 500, suggesting a longer left tail (more extreme negative returns). Kurtosis values highlight leptokurtic distributions, particularly in the S&P 500, where extreme returns are more likely. For the Renko strategy, skewness is consistently positive across all indices, and kurtosis values are particularly high in the S&P 500, suggesting a higher likelihood of extreme positive returns. These distribution properties emphasize the potential for both substantial gains and losses, which necessitates careful risk management.

Profitability analysis reveals that both strategies experience more profitable months than losing months. For the Kagi strategy, the average profitable-month returns range from 0.0113 (CSI 100) to 0.0147 (CSI 300), while the average losing-month returns range from −0.0070 (S&P 500) to −0.0121 (CSI 500). The percentage of negative observations is lower in the S&P 500 (20.5%) compared to the CSI indices. The Renko strategy exhibits similar trends, with slightly better performance in the CSI indices. To quantify what drives the monthly means, we decompose the mean as $\mu \approx (1-p)\mu_+ + p\mu_-$, where p is the fraction of losing months, μ_+ the average profitable-month return, and μ_- the average losing-month return. For Kagi in the S&P 500, $(1 - 0.205) \times 0.0135 + 0.205 \times (-0.0070) \approx 0.0093$, exactly matching the reported mean; the implied payoff ratio $\mu_+/|\mu_-| \approx 1.9$ indicates that gains in winning months materially exceed losses in losing months. A similar check for Renko in the S&P 500 yields $(1 - 0.208) \times 0.0130 + 0.208 \times (-0.0067) \approx 0.0089$. These diagnostics show that both a high win rate and favorable payoff asymmetry underpin profitability—useful for stress-testing how shifts in the loss frequency p or in $|\mu_-|$ would affect the mean.

Risk-adjusted performance metrics corroborate these findings. Kagi attains higher Sharpe ratios and Jensen's alpha in the S&P 500 and CSI 300, whereas Renko posts higher Sharpe ratios in the CSI 100, CSI 200, and CSI 500. We report Modigliani RAP in excess-return form, $RAP = SR \times \sigma_{benchmark}$, which preserves the same cross-market ranking: Kagi reaches its highest RAP in CSI 300 at 0.0364, while Renko's RAP is relatively stable across the CSI indices at about 0.027–0.029. Jensen's alpha closely tracks mean excess returns—for the S&P 500, Kagi is 0.0094 versus a mean of 0.0093, and Renko is 0.0087 versus 0.0089—consistent with near-market-neutral exposure and low betas. To substantiate neutrality and enable formal Sharpe comparisons, we recommend reporting factor betas (market, size, value, momentum) and using Jobson–Korkie, Ledoit–Wolf, or bootstrap confidence intervals.

Taken together, the cross-market patterns are consistent with a market-efficiency interpretation: Kagi tends to exploit finer price reversals in the highly liquid and efficient S&P 500 and CSI 300, while Renko is relatively more competitive than Kagi across several CSI segments, namely CSI 100, CSI 200, and CSI 500. This interpretation is descriptive rather than causal. To assess stability, we recommend simple regime splits by volatility level and by crisis versus tranquil periods, together with subperiod tests or rolling-window Sharpe and alpha, to determine whether these rankings persist or are regime dependent. These diagnostics are directly relevant for deployment timing and capital allocation.

Table 2 reports gross performance; transaction costs and execution frictions are not incorporated here. Given the potentially high turnover of brick-based rules, a comprehensive assessment requires explicit transaction-cost modeling and execution considerations. We address these issues subsequently and also report gross returns for comparability.

In sum, both Kagi and Renko constructions deliver statistically significant monthly excess returns across indices. Kagi tends to lead in more efficient markets such as the S&P 500, whereas Renko is relatively stronger than Kagi across several CSI indices. Risk-adjusted metrics (Sharpe, Modigliani RAP, Jensen's alpha) indicate that returns are commensurate with risk. At the same time, the documented skewness and kurtosis—especially in the S&P 500—underscore the importance of risk management; transaction costs should be incorporated to gauge real-world performance.

Table 2. Monthly excess returns of the Kagi and Renko pairs trading strategy without transaction costs.

Market Index	S&P 500	CSI 300	CSI 100	CSI 200	CSI 500
Panel A: Distribution of monthly excess returns of Kagi constructions.					
Mean	0.0093	0.0071	0.0047	0.0054	0.0052
Standard error	0.0008	0.0011	0.0010	0.0011	0.0012
t-Statistics	12.3469	6.6946	4.7586	4.8180	4.3856
P-Value	0.0000	0.0000	0.0000	0.0000	0.0000
Median	0.0084	0.0064	0.0052	0.0047	0.0059
Standard deviation	0.0140	0.0158	0.0143	0.0158	0.0167
Skewness	0.5024	0.2801	-0.4147	0.6116	-0.7431
Kurtosis	5.3955	1.2752	1.8484	1.1264	2.5630
Minimum	-0.0682	-0.0415	-0.0458	-0.0311	-0.0757
Maximum	0.0727	0.0696	0.0556	0.0602	0.0502
Average profitable month	0.0135	0.0147	0.0113	0.0140	0.0143
Average losing month	-0.0070	-0.0105	-0.0117	-0.0103	-0.0121
Negative observations (%)	20.5	30.2	28.6	35.4	34.3
Sharpe ratio	0.6676	0.4493	0.3284	0.3424	0.3117
Modigliani RAP	0.0298	0.0364	0.0263	0.0255	0.0232
Jensen's alpha	0.0094	0.0071	0.0047	0.0054	0.0052
Panel B: Distribution of monthly excess returns of Renko constructions.					
Mean	0.0089	0.0057	0.0053	0.0058	0.0065
Standard error	0.0008	0.0011	0.0010	0.0011	0.0012
t-Statistics	11.2422	5.0275	5.3062	5.3879	5.5003
P-Value	0.0000	0.0000	0.0000	0.0000	0.0000
Median	0.0069	0.0063	0.0045	0.0050	0.0055
Standard deviation	0.0147	0.0169	0.0145	0.0151	0.0166
Skewness	2.2261	0.3860	0.5216	0.0174	0.0320
Kurtosis	13.2497	2.6970	2.1147	1.7205	1.8052
Minimum	-0.0306	-0.0506	-0.0417	-0.0598	-0.0616
Maximum	0.1227	0.0900	0.0659	0.0529	0.0588
Average profitable month	0.0130	0.0150	0.0126	0.0141	0.0148
Average losing month	-0.0067	-0.0115	-0.0093	-0.0091	-0.0105
Negative observations (%)	20.8	35.1	33.3	35.9	32.8
Sharpe ratio	0.6079	0.3374	0.3662	0.3829	0.3909
Modigliani RAP	0.0272	0.0273	0.0293	0.0286	0.0292
Jensen's alpha	0.0087	0.0056	0.0055	0.0058	0.0065

Note: This table presents the monthly excess returns of the Kagi and Renko pairs trading strategies across different market indices, without accounting for transaction costs. Panel A reports the statistical distribution of excess returns

for Kagi constructions, while Panel B provides the corresponding metrics for Renko constructions. The Modigliani risk-adjusted performance (RAP) provides a comprehensive evaluation of a strategy's performance by adjusting for risk. It is computed as the product of the Sharpe ratio and the standard deviation of the benchmark returns. This metric facilitates a direct comparison between the strategy's risk-adjusted performance and that of the benchmark. Results indicate statistical significance (p-value < 0.05) across all indices, highlighting the robustness of the strategies. Differences in Sharpe ratio, Modigliani RAP, and Jensen's alpha between Kagi and Renko constructions reflect variations in their risk-adjusted returns and strategy-specific characteristics.

The following section evaluates monthly excess returns for Kagi- and Renko-based pairs trading including transaction costs (Table 3) and contrasts them with the gross results in Table 2. We assess performance across multiple indices and compare headline profitability, statistical significance, and risk-adjusted returns under realistic trading frictions.

After costs, both strategies continue to post positive mean monthly excess returns across all indices, although magnitudes and test statistics decline materially. For Kagi, means range from 0.0009 in CSI 500 to 0.0052 in S&P 500. Statistical significance remains at the 1% level in S&P 500, and in CSI 300, but not in CSI 100, CSI 200, or CSI 500, respectively. For Renko, means span 0.0031 in CSI 300 to 0.0064 in S&P 500 and are statistically significant across all indices. These results imply statistically robust net profitability in the most liquid venues—strongest in S&P 500 and, though economically smaller, still significant in CSI 300—whereas for Kagi the net means in CSI 100, CSI 200, and CSI 500 are statistically indistinguishable from zero, reversing the inference from Table 2.

Transaction costs have a pronounced impact on the profitability of the strategies, leading to a reduction in mean returns. For the Kagi strategy, mean returns in the S&P 500 index drop by approximately 44%, from 0.0093 (without costs) to 0.0052 (with costs). In the CSI 500 index, the reduction is even more substantial, at 83%. The Renko strategy shows a smaller reduction in mean returns, with the S&P 500 index decreasing by 28% and the CSI 500 index by 45%. These results indicate that transaction costs significantly affect both strategies' profitability, with the Kagi strategy being more adversely impacted than the Renko strategy. Despite these reductions, both strategies remain profitable in the S&P 500 and CSI 300 indices after accounting for transaction costs, although profitability diminishes in other indices. The larger percentage drop for Kagi—most pronounced in CSI 200 and CSI 500—likely reflects higher turnover: its reversal-sensitive rules trigger more trades and therefore incur greater fees.

The statistical significance of the returns is also influenced by transaction costs. For the Kagi strategy, the t-statistics for the CSI 100, CSI 200, and CSI 500 indices drop below the threshold for statistical significance, with p-values exceeding 0.05. This indicates that the observed mean excess returns in these markets may not be reliably different from zero. In contrast, the Renko strategy retains statistical significance across all indices, with t-statistics remaining above 2 and p-values below 0.05. This suggests that the Renko strategy demonstrates greater robustness to transaction costs in terms of maintaining statistically significant returns.

Risk-adjusted performance metrics also highlight the negative impact of transaction costs. Sharpe ratios for both strategies decrease across all indices compared to those without transaction costs. For the Kagi strategy, the Sharpe ratio in the S&P 500 index drops from 0.6676 to 0.3969, while for the Renko strategy, it decreases from 0.6079 to 0.4483. Modigliani risk-adjusted performance (RAP) values also decline, with the Kagi strategy showing significant reductions, such as in the CSI 500 index where the RAP drops from 0.0232 to 0.0040. Similarly, Jensen's alpha values for both strategies decrease, with the Kagi strategy in the S&P 500 index falling from 0.0094 to 0.0053, and the Renko strategy dropping from 0.0087 to 0.0061. Overall, the Renko strategy maintains relatively higher risk-adjusted performance metrics compared to the Kagi strategy, suggesting better adaptability to transaction costs.

Transaction costs also increase the frequency of losing months for both strategies. For the Kagi strategy, the percentage of negative observations rises across all indices, with the S&P 500 increasing from 20.5% (without costs) to 32.2% (with costs). The Renko strategy experiences a smaller increase, with negative observations in the S&P 500 rising from 20.8% to 28.7%. Average profitable month returns decrease for both strategies, and average losing month returns become more negative. The Kagi strategy shows a larger reduction in average profitable month returns compared to the Renko strategy, reflecting its greater sensitivity to transaction costs.

The inclusion of transaction costs does not significantly alter the distribution characteristics of the returns. Skewness values remain similar or slightly decrease for both strategies, indicating relatively stable distribution shapes. Kurtosis values continue to suggest the presence of fat tails in certain indices, particularly in the S&P 500, where extreme returns remain possible. A notable change appears in Renko for CSI 200, where skewness turns slightly negative to about −0.086,

indicating occasional larger left-tail months after costs. These patterns underscore the need for continued tail-risk management even when transaction costs are incorporated.

Comparative analysis between the Kagi and Renko strategies highlights the Renko strategy's greater resilience to transaction costs. While both strategies experience reduced profitability and risk-adjusted returns, the Renko strategy retains statistically significant excess returns and better performance metrics across all indices. This may be attributed to the structural differences between the two strategies, as the Renko strategy's emphasis on significant price movements likely generates fewer trades, resulting in lower transaction costs. In contrast, the Kagi strategy's sensitivity to price reversals may lead to more frequent trading and higher cumulative transaction costs.

From an implementation standpoint, incorporating realistic costs is decisive for capital allocation. Choosing parameters that reduce turnover—such as larger bricks and stricter signal filters—and executing trades cost-efficiently can materially improve net performance. Strategy–market matching also matters: the S&P 500 and CSI 300 remain the most favorable venues after costs, particularly for Renko. As a rule of thumb, when expected gross monthly returns approach the per-pair round-trip cost—about 0.30 percent per-trade fee—disciplining turnover becomes the primary lever for preserving net returns.

In sum, transaction costs materially compress profitability and risk-adjusted performance for both Kagi and Renko. Kagi is more adversely affected—especially in CSI 100, CSI 200, and CSI 500 where net means lose statistical significance—while Renko remains significant across all indices and retains stronger risk-adjusted metrics in most cases. Evaluating strategies on a net basis and adapting design and deployment to market conditions is therefore essential for practical profitability. The continued leadership of the S&P 500 and CSI 300 after costs is consistent with liquidity and execution quality being primary drivers of deployable alpha for brick-based pairs strategies, although we do not claim causality.

Table 3. Monthly excess returns of the Kagi and Renko pairs trading strategy with transaction costs.

Market Index	S&P 500	CSI 300	CSI 100	CSI 200	CSI 500
Panel A: Distribution of monthly excess returns of Kagi constructions.					
Mean	0.0052	0.0031	0.0016	0.0018	0.0009
Standard error	0.0007	0.0010	0.0010	0.0011	0.0012

Market Index	S&P 500	CSI 300	CSI 100	CSI 200	CSI 500
Panel A: Distribution of monthly excess returns of Kagi constructions.					
t-Statistics	7.3398	3.0260	1.5957	1.6056	0.7586
P-Value	0.0000	0.0028	0.1121	0.1100	0.4490
Median	0.0039	0.0023	0.0021	0.0015	0.0022
Standard deviation	0.0131	0.0155	0.0142	0.0155	0.0164
Skewness	0.1337	0.1796	-0.5787	0.5465	-0.8676
Kurtosis	5.5313	1.2560	2.2679	1.1113	2.6972
Minimum	-0.0732	-0.0448	-0.0533	-0.0333	-0.0794
Maximum	0.0607	0.0630	0.0500	0.0559	0.0417
Average profitable month	0.0111	0.0124	0.0104	0.0126	0.0122
Average losing month	-0.0072	-0.0115	-0.0104	-0.0110	-0.0129
Negative observations (%)	32.2	38.7	42.4	46.0	45.0
Sharpe ratio	0.3969	0.2031	0.1101	0.1141	0.0539
Modigliani RAP	0.0177	0.0165	0.0088	0.0085	0.0040
Jensen's alpha	0.0053	0.0032	0.0016	0.0018	0.0009
Panel B: Distribution of monthly excess returns of Renko constructions.					
Mean	0.0064	0.0031	0.0033	0.0034	0.0036
Standard error	0.0008	0.0011	0.0010	0.0011	0.0012
t-Statistics	8.2907	2.8333	3.3946	3.2542	3.1214
P-Value	0.0000	0.0050	0.0008	0.0013	0.0021
Median	0.0045	0.0038	0.0027	0.0026	0.0034
Standard deviation	0.0142	0.0166	0.0143	0.0149	0.0162
Skewness	2.0458	0.3201	0.3691	-0.0859	-0.0575
Kurtosis	12.5595	2.7411	2.1262	2.0463	1.8345
Minimum	-0.0354	-0.0536	-0.0446	-0.0643	-0.0631
Maximum	0.1155	0.0856	0.0618	0.0499	0.0537
Average profitable month	0.0117	0.0131	0.0115	0.0135	0.0133
Average losing month	-0.0069	-0.0126	-0.0098	-0.0093	-0.0110
Negative observations (%)	28.7	38.7	38.1	44.0	39.9
Sharpe ratio	0.4483	0.1902	0.2343	0.2313	0.2218
Modigliani RAP	0.0200	0.0154	0.0187	0.0172	0.0165
Jensen's alpha	0.0061	0.0031	0.0035	0.0034	0.0036

Note: This table presents the monthly excess returns of the Kagi and Renko pairs trading strategies across different market indices, with accounting for transaction costs. Panel A reports the statistical distribution of excess returns for Kagi constructions, while Panel B provides the corresponding metrics for Renko constructions. The Modigliani risk-adjusted performance (RAP) provides a comprehensive evaluation of a strategy's performance by adjusting for risk. It is computed as the product of the Sharpe ratio and the standard deviation of the benchmark returns. This metric facilitates a direct comparison between the strategy's risk-adjusted performance and that of the benchmark. Results

indicate statistical significance (p-value < 0.05) across all indices, highlighting the robustness of the strategies. Differences in Sharpe ratio, Modigliani RAP, and Jensen's alpha between Kagi and Renko constructions reflect variations in their risk-adjusted returns and strategy-specific characteristics.

Figure 4. Strategy historical performance for top 20 pairs portfolio before transaction cost.
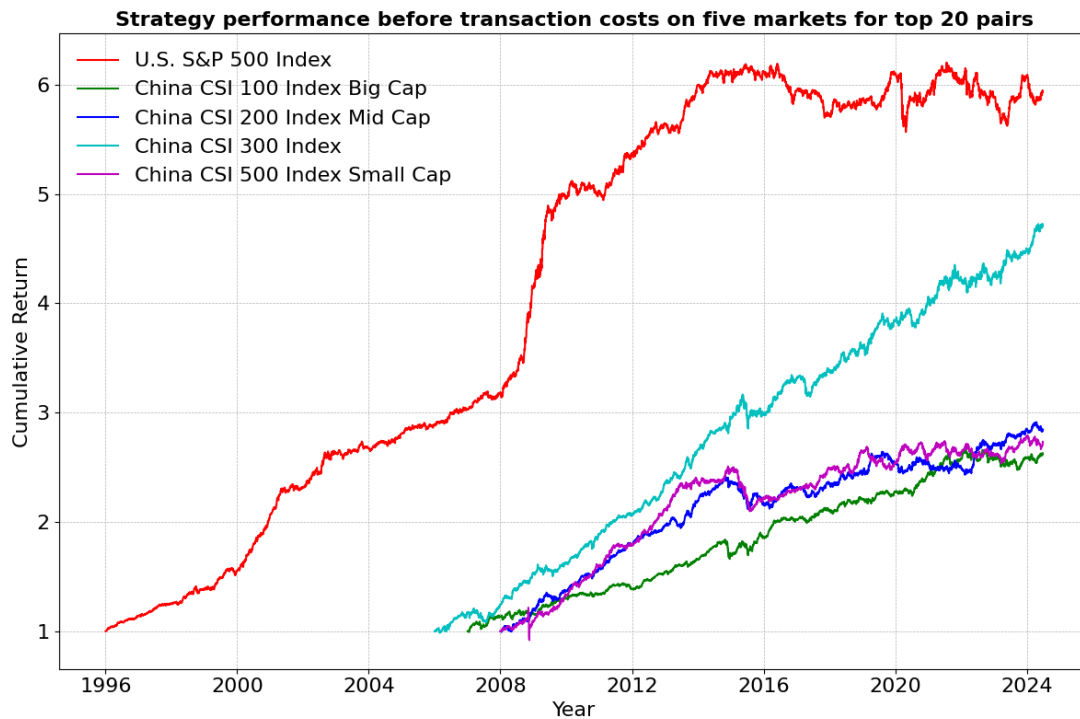
Note: The strategies start on different dates based on the availability of data for each stock index. The U.S. S&P 500 Index starts from January 1996, the China CSI 300 Index begins in January 2006, the China CSI 100 Index starts in January 2007, and both the China CSI 200 Index and China CSI 500 Index start from January 2008. All cumulative returns are calculated from these respective starting points to ensure accurate representation of out-of-sample performance.

Figure 5 reports 36-month rolling Sharpe ratios. The U.S. S&P 500 series is the most stable and generally the highest prior to 2010, with peaks above 1.0 and a broad 0.6–0.9 range; it softens after 2011, dips to about 0.5–0.6 in 2011–2013, and declines further after 2016, reaching roughly 0.4 by 2023 before a small rebound in 2024. This persistence and relative stability are consistent with Tables 2 and 3: the U.S. venue delivers the strongest risk-adjusted returns on both a gross and a net basis, even after cost compression.

For China, CSI 100 hovers around 0.5 from 2008 to 2021 but then falls sharply to roughly 0.15 by 2024. CSI 200 is visibly more volatile, reaching 0.7–0.8 around 2010–2011, showing a brief rebound in 2020–2021, and trending down to about 0.3 thereafter. CSI 300 is

comparatively steady near 0.4–0.8 through 2018 and then weakens, approaching zero by 2023 and slightly below thereafter. CSI 500 is the most cyclical—very strong in 2008–2015 around 0.9–1.1, followed by a steep decline, turning negative around 2022 and hovering near zero in 2023 with only a mild uptick in 2024. Taken together, the Chinese series display clear regime dependence: strength in 2008–2015, a mixed rebound around 2020–2021, and broad weakening since 2021/2022, which dovetails with the net-of-cost results where CSI 300 remains deployable while small- and mid-cap universes erode more.

Two practical implications follow. First, conditioning exposure on market state matters: the S&P 500 and, within China, CSI 300 warrant higher or steadier allocations, while CSI 100/200/500 exposures are better made state-contingent and turnover-aware. Second, the rolling-Sharpe evidence aligns with the cost mechanism in Table 3—segments that trade more or face tighter liquidity experience larger net performance decay—so parameter choices that limit turnover (larger bricks, stricter filters) are likely to preserve risk-adjusted returns.

Figure 5. Three-year rolling Sharpe ratios for five market universes: S&P 500 (blue), CSI 100 (red), CSI 200 (orange), CSI 300 (green), and CSI 500 (purple).

Note: Sharpe ratios are computed from monthly excess returns using a 36-month rolling window; series begin once 36 observations are available. Because windows overlap, the figure is descriptive; inference should rely on separate tests (e.g., subperiod or regime splits).

5.2 Risk Adjusted Performance

This section evaluates risk-adjusted performance for Kagi and Renko before and after transaction costs using lower-partial-moment (LPM) and drawdown measures (Table 4). LPM metrics—Omega, Sortino, and Kappa-3—focus on downside deviations relative to a target return and are therefore informative under non-normal return distributions, a feature documented for our series and in prior work. This approach contrasts with the Sharpe ratio, which treats positive and negative deviations symmetrically, potentially underestimating risk when return distributions are non-normal—a characteristic observed in our return series (Eling, 2008). This design lets us separate "how much return" from "how that return is earned when losses matter most."

The tail-sensitive reward indicators point to a clear size effect. Before costs, Kagi delivers the strongest reward-to-risk profile in the large-cap CSI 300 (Omega 3.25, Sortino 0.53, Kappa-3 0.66), clearly outstripping its Renko counterpart. After commissions and fees, Kagi's edge narrows sharply—its CSI 300 Omega falls by about 48 percent to 1.71—yet within Kagi's China sleeves CSI 300 remains the top performer. By contrast, in the mid- and small-capitalization universes (CSI 100, 200, 500) the Renko construction is structurally more resilient: although costs still erase roughly 30–37 percent of the pre-cost Omega, the post-cost levels (around 1.8–1.9) remain materially above those for Kagi (around 1.1–1.4). This pattern is consistent with Renko's brick-width filter sacrificing some upside in calm markets but curbing noise-induced over-trading when bid–ask spreads widen or depth thins—conditions that disproportionately affect the smaller CSI sleeves.

Drawdown metrics reinforce the size-dependent narrative. Before costs, maximum peak-to-trough losses are modest—Kagi roughly −7 to −16 percent, Renko as low as −3.23 percent in the S&P 500—and the recovery-weighted ratios split cleanly: Sterling exceeds one in every sleeve; Calmar exceeds one only for Kagi in the S&P 500 and CSI 300 and for Renko in the S&P 500; Burke exceeds one only for Renko in the S&P 500. After costs, adverse excursions increase non-linearly, especially for Kagi in CSI 200 and CSI 500, where maximum drawdown more than doubles to about −26 and −33 percent and Calmar collapses to 0.08 and 0.03. Renko suffers smaller proportional deteriorations: in CSI 100, CSI 200, and CSI 500 the post-cost Calmar remains clearly positive, roughly 0.27 to 0.46, which preserves some compounding capacity. CSI 300 again stands out. Kagi's post-cost maximum drawdown is contained at −10.5 percent and

Calmar holds at 0.37, while Renko records −18.2 percent and 0.21. A simple check is consistent with the table: the Renko S&P 500 net monthly mean is about 0.0064, which annualizes to roughly 7.7 percent; with a 4.1 percent maximum drawdown the implied Calmar is near 1.9, in line with the reported value. Overall, the data show that higher turnover and tighter liquidity in mid- and small-cap universes make drawdowns and recovery ratios far more sensitive to costs, while constructions that restrain trading intensity better defend the left tail after fees.

Taken together, the evidence supports a "horses for courses" prescription. In sleeves where trading is easier and execution frictions are lower—most clearly in the U.S. and, within China, in CSI 300—Kagi's direction-flip logic can deliver a superior left-tail payoff despite higher turnover. In the more frictional mid- and small-cap sleeves—CSI 100, CSI 200, and CSI 500— the Renko algorithm's absolute-move trigger tempers trading intensity and better preserves both tail and drawdown efficiency once realistic costs are imposed. For portfolio construction, rather than imposing hard cut-offs that our net metrics rarely meet in China, a practical rule is to prioritize sleeves with higher post-cost Calmar and Burke and to allocate Kagi only where it actually clears a modest recovery profile. Under our results, that points to Kagi in CSI 300 and Renko in CSI 100/200/500, with brick widths calibrated to recent spread volatility (for example, a volatility-scaled factor around unity) to control turnover.

Mechanistically, Kagi's direction-flip logic reacts to smaller reversals and trades more often, so costs bite harder; Renko's absolute-move trigger trades less, sacrificing some upside in calm regimes but better defending the left tail when liquidity deteriorates. Reporting turnover and average holding period by sleeve would validate this channel empirically; fee drag should co-vary positively with turnover after controlling for index effects.

For implementation, parameter choices that limit turnover—larger bricks, stricter signal filters, or minimum dwelling times—can materially improve net risk-adjusted performance in cost-sensitive sleeves. Strategy–market matching matters: the S&P 500 and CSI 300 remain the most deployable after costs, particularly for Renko in the U.S. and for Kagi in CSI 300; small- and mid-cap sleeves warrant state-contingent exposure and tighter execution control.

In sum, both constructions are robust on a gross basis, but net outcomes diverge with frictions. Renko maintains higher Omega and Sortino and more favorable drawdowns in most China sleeves after costs, while Kagi remains competitive—and often superior—in CSI 300.

These findings argue for evaluating strategies strictly net of costs and for tailoring the brick construction and parameters to market microstructure so that deployable, downside-aware performance is preserved.

Table 4. Overview of risk-adjusted performance.

	Lower partial moments measures			Drawdown measures			
	Omega	Sortino ratio	Kappa 3	Max Drawdown	Calmar ratio	Sterling ratio	Burke ratio
Panel A-I: Monthly excess returns of Kagi constructions before transaction costs							
S&P 500	7.5046	0.7862	0.8682	-0.0699	1.6851	10.9356	0.7601
CSI 300	3.2524	0.5281	0.6596	-0.0758	1.1692	5.3884	0.4030
CSI 100	2.4057	0.2957	0.3626	-0.0800	0.7246	2.8840	0.2049
CSI 200	2.4814	0.4286	0.5341	-0.1130	0.5907	1.8932	0.1351
CSI 500	2.2482	0.2985	0.3218	-0.1562	0.4111	1.6861	0.1043
Panel A-II: Monthly excess returns of Renko constructions before transaction costs							
S&P 500	7.4142	0.9216	1.2333	-0.0323	3.4953	14.0857	1.0432
CSI 300	2.4080	0.3828	0.4490	-0.1246	0.5653	1.8649	0.1172
CSI 100	2.7202	0.4380	0.5110	-0.0680	0.9673	3.2316	0.2280
CSI 200	2.7755	0.4558	0.4799	-0.0867	0.8273	3.4911	0.2358
CSI 500	2.8727	0.4375	0.4883	-0.0894	0.9009	2.7775	0.2097
Panel B-I: Monthly excess returns of Kagi constructions after transaction costs							
S&P 500	3.2293	0.4567	0.4394	-0.0889	0.7199	2.6607	0.1435
CSI 300	1.7068	0.2132	0.2465	-0.1049	0.3664	1.2801	0.0812
CSI 100	1.3564	0.1029	0.1061	-0.1049	0.1809	0.6315	0.0361
CSI 200	1.3501	0.1283	0.1450	-0.2639	0.0811	0.1625	0.0113
CSI 500	1.1524	0.0489	0.0491	-0.3323	0.0321	0.0658	0.0044
Panel B-II: Monthly excess returns of Renko constructions after transaction costs							
S&P 500	4.2420	0.6408	0.7555	-0.0410	1.9302	7.7781	0.4879
CSI 300	1.6463	0.1972	0.2262	-0.1821	0.2111	0.7848	0.0450
CSI 100	1.8947	0.2590	0.2881	-0.0897	0.4562	1.5515	0.1005
CSI 200	1.8401	0.2638	0.2601	-0.1125	0.3749	1.5145	0.0952
CSI 500	1.8183	0.2356	0.2490	-0.1652	0.2662	0.7445	0.0491

Note: This table summarizes risk-adjusted performance metrics for monthly excess returns of Kagi and Renko constructions, both before and after transaction costs. Metrics include Omega, Sortino ratio, Kappa 3, Max Drawdown, Calmar ratio, Sterling ratio, and Burke ratio, evaluated for indices like S&P 500, CSI 300, CSI 100, CSI 200, and CSI 500.

5.3 Sub-period Performance Analysis

We analyse sub-period performance for the Kagi and Renko pairs-trading strategies in the Chinese market using Table 5 and Figure 6. The sample is partitioned into nine economically motivated regimes: pre-GFC (Jan 2005–Dec 2006), GFC (Jan 2007–Dec 2008), post-GFC (Jan 2009–Dec 2010), pre-bullish and non-bullish phases (Jan 2011–Dec 2013), bullish period (Jan 2014–May 2015), bearish period (Jun 2015–Dec 2016), pre-COVID (Jan 2017–Dec 2019), COVID (Jan 2020–Dec 2022), and post-COVID (Jan 2023–Jun 2024). This exogenous partition enables like-for-like comparisons across distinct market states and mitigates hindsight bias. Coverage varies by index: CSI 300 is available from 2005, whereas CSI 100, CSI 200 and CSI 500 begin in 2007, hence the early cells are empty in Table 5. All statistics are based on monthly excess returns and are reported both gross and net of transaction costs.

Before costs, both rules delivered double-digit annualized returns on CSI 300 during the pre-GFC boom: monthly means were about 1.3 percent for Kagi and for Renko. In the GFC window of 2007–08, CSI 200 was particularly strong, with mean monthly gains of 1.55 percent under Kagi and 1.41 percent under Renko. Renko's Sharpe rose to 0.80–0.90 on CSI 200 and CSI 500, whereas Kagi's peaked near 0.55 on CSI 200 and was lower elsewhere. This pattern is consistent with unusually high signal-to-noise in spread moves when cross-sectional valuation dispersion widened, but it was more pronounced under the Renko construction.

Following the bubble's burst and the global sell-off, performance moderated. In 2009–10, average monthly returns settled within a wider band—about 0.9 to 1.6 percent for Kagi across sleeves and roughly 0.4 to 1.5 percent for Renko—while Sharpe ratios generally moved into the 0.5 to 1.1 range, depending on the index. Small caps proved most resilient in this window (Kagi on CSI 500 reached 1.61 percent with a Sharpe near 1.1), whereas CSI 300 under Kagi was closer to 0.88 percent with a Sharpe just below 0.5. A second compression emerged during the policy-driven sideways phase of 2011–13: on CSI 300, Renko held at about half a percentage point per month, whereas Kagi stayed near one percent, a split consistent with faster signal turnover for Kagi noted in the full-sample analysis.

The late-2014 to mid-2015 bull run did not yield blanket Kagi dominance. Kagi leads on CSI 300, CSI 100, and CSI 200, but Renko is decisively ahead on CSI 500: Renko posts 0.51% per month with a Sharpe of 0.31, whereas Kagi records −0.26% and −0.15. After the bubble burst

in 2015–2016, Kagi's monthly means compress toward zero, roughly 0.18% on CSI 200 and 0.09% on CSI 500, and its Sharpe ratios fall into the 0.11 to 0.34 range, although CSI 100 remains around 0.50. Renko holds up better, delivering about 0.74% per month on CSI 300 with a Sharpe near 0.58 and staying close to 0.60 on CSI 100 and CSI 200, while CSI 500 comes in lower at 0.42.

The pre-COVID expansion from 2017 to 2019 shows a gradual erosion for both constructions. Mean returns settle in the 25 to 45 basis-point range, with Renko delivering slightly stronger risk metrics in the mid- and small-cap sleeves, while Kagi retains a modest edge on the blue-chip CSI 300. The pandemic years from 2020 to 2022 accentuate this split. Renko flattens but remains marginally positive on three of the four indices, whereas Kagi stays small-positive across the board, including CSI 300. The pattern carries into the post-COVID window through mid-2024, with only a faint rebound visible for Kagi on CSI 300. When transaction costs are included, the divergence is sharper: Kagi turns negative on CSI 300 during 2020 to 2022, while Renko keeps a narrow lead in the more frictional sleeves.

Transaction costs alter the hierarchy in predictable but material ways. On CSI 300, net returns remain positive in eight of nine windows for Kagi and seven of nine for Renko, but the margins are thin and do not consistently support strong inference. The large-cap sleeve still offers enough depth for Kagi to preserve a modest post-2023 Sharpe of 0.26. Across the full set of windows, the best net Sharpe on CSI 300 is about 0.57 for Renko during 2007–08, while Kagi's best net reading is about 0.46 in 2011–13; both are well below the gross Sharpe of 0.76 that Kagi achieved in 2011–13, underscoring the compressive effect of costs.

The mid-cap CSI 200 and small-cap CSI 500 become largely unattractive for Kagi once commissions are deducted, especially after 2015 when several windows turn negative and Sharpe ratios hover near zero or slip into the red. In stress phases, CSI 500 is hit hardest, with negative means and Sharpe readings that drop as low as about −0.26 during COVID, while CSI 200 weakens to small negatives with Sharpe modestly below zero. Renko copes better. Its absolute-move trigger reduces churn and caps slippage in thin order books. Even in the 2015–2016 bear window Renko retains about fifty basis points per month on CSI 200 and roughly forty-four basis points on CSI 500, with Sharpe near 0.44 and 0.28 respectively.

With costs included, COVID provides the sharpest contrast. Kagi turns negative or negligible during 2020–2022, posting roughly −14 basis points per month on CSI 300, −19 on CSI 200, and −36 on CSI 500, with only a marginal 3 on CSI 100. Renko holds up better: net averages are about 36 basis points on CSI 100 and 19 on CSI 200, and the corresponding Sharpe ratios are positive on these two sleeves, although CSI 300 and CSI 500 slip slightly negative. In the post-COVID window through mid-2024, the spread advantage compresses further: Renko hovers near break-even but remains slightly below zero across indices, while Kagi stays negative on all sleeves except CSI 300, which edges back into modestly positive territory.

The sub-period results support a segmented implementation. In the deep, lower-friction CSI 300 sleeve, Kagi remains the preferred engine: execution quality contains slippage and allows fast reversal recycling to translate into superior post-cost outcomes. In the more friction-sensitive mid- and small-cap sleeves of CSI 200 and CSI 500, Renko is superior, particularly in stress regimes when wider spreads and shallow depth amplify fee drag on higher-turnover rules. For CSI 100, which is liquid but still shows greater post-cost sensitivity for Kagi, Renko generally retains a net edge. Within the Renko framework, brick width should be volatility-aware: broader bricks in boom-to-bust transitions cut whipsaws and preserve crisis alpha, while narrower bricks in extended bull phases capture incremental mean reversion without giving up upside.

In short, the statistical-arbitrage edge in Chinese equity pairs is both regime-dependent and cost-sensitive. Within China, depth and execution quality in the CSI 300 keep the Kagi construction competitive on a net basis across many regimes, whereas the more friction-prone mid- and small-cap sleeves favor the Renko filter, especially when turbulence rises or liquidity thins. A cost-aware, state-contingent allocation—tilting toward Kagi in CSI 300 and toward Renko in CSI 100, CSI 200, and CSI 500—combined with volatility-scaled sizing, is therefore advisable to preserve the net absolute-return profile documented in Tables 4 and 5.

Table 5. Sub-Period performance of pairs trading strategies for Chinese market.

Market	Sub-Period	Pre-Fin.C.	In- Fin.C.	Post-Fin.C.	Pre-B.N.B.	In-Bullish	In-Bearish	Pre-Cov.	In-Cov.	Post-Cov.
		Jan 2005-Dec 2006	Jan 2007-Dec 2008	Jan 2009-Dec 2010	Jan 2011-Dec 2013	Jan 2014-May 2015	June 2015-Dec 2016	Jan 2017-Dec 2019	Jan 2020-Dec 2022	Jan 2023-June 2024
Panel A-I: Monthly excess returns of Kagi constructions before transaction costs										
CSI 300	Mean	0.0132	0.0116	0.0088	0.0097	0.0083	0.0042	0.0042	0.0029	0.0056
	Sharpe	0.6345	0.4467	0.4939	0.7579	0.5178	0.3355	0.3151	0.2465	0.6304
CSI 100	Mean	-	0.0063	0.0060	0.0060	0.0046	0.0068	0.0033	0.0036	0.0010
	Sharpe	-	0.2536	0.5824	0.5385	0.2375	0.5007	0.3895	0.2479	0.0955
CSI 200	Mean	-	0.0155	0.0115	0.0093	0.0013	0.0018	0.0027	0.0019	0.0028
	Sharpe	-	0.5511	0.6265	0.7632	0.0933	0.1066	0.2215	0.1179	0.3498
CSI 500	Mean	-	0.0078	0.0161	0.0110	-0.0026	0.0009	0.0030	0.0008	0.0025
	Sharpe	-	0.2394	1.1170	0.9150	-0.1498	0.0544	0.2018	0.0544	0.2168
Panel A-II: Monthly excess returns of Renko constructions before transaction costs										
CSI 300	Mean	0.0131	0.0130	0.0124	0.0054	0.0035	0.0074	0.0025	0.0002	0.0002
	Sharpe	0.3553	0.7363	0.6505	0.5474	0.2185	0.5763	0.1895	0.0145	0.0126
CSI 100	Mean	-	0.0146	0.0037	0.0054	0.0013	0.0097	0.0018	0.0057	0.0004
	Sharpe	-	0.6575	0.2090	0.5136	0.0904	0.6640	0.2041	0.4339	0.0387
CSI 200	Mean	-	0.0141	0.0118	0.0054	0.0010	0.0072	0.0044	0.0043	0.0016
	Sharpe	-	0.8048	0.5954	0.5134	0.0531	0.6168	0.3038	0.2824	0.1581
CSI 500	Mean	-	0.0177	0.0146	0.0104	0.0051	0.0068	0.0025	-0.0002	0.0025
	Sharpe	-	0.9042	0.8245	0.7753	0.3144	0.4171	0.2393	-0.0108	0.1549
Panel B-I: Monthly excess returns of Kagi constructions after transaction costs										
CSI 300	Mean	0.0094	0.0069	0.0052	0.0057	0.0039	0.0009	0.0004	-0.0014	0.0022
	Sharpe	0.4646	0.2665	0.2951	0.4648	0.2610	0.0701	0.0331	-0.1215	0.2620
CSI 100	Mean	-	0.0024	0.0033	0.0030	0.0007	0.0043	0.0002	0.0003	-0.0016
	Sharpe	-	0.0986	0.3156	0.2744	0.0315	0.3093	0.0301	0.0232	-0.1572
CSI 200	Mean	-	0.0115	0.0079	0.0054	-0.0027	-0.0010	-0.0009	-0.0019	-0.0003
	Sharpe	-	0.4183	0.4344	0.4555	-0.1895	-0.0588	-0.0776	-0.1233	-0.0371
CSI 500	Mean	-	0.0027	0.0113	0.0064	-0.0069	-0.0023	-0.0013	-0.0036	-0.0013
	Sharpe	-	0.0858	0.7989	0.5452	-0.3863	-0.1369	-0.0899	-0.2550	-0.1213
Panel B-II: Monthly excess returns of Renko constructions after transaction costs										
CSI 300	Mean	0.0106	0.0099	0.0099	0.0029	0.0006	0.0053	0.0001	-0.0024	-0.0019
	Sharpe	0.2916	0.5698	0.5283	0.3064	0.0352	0.3975	0.0045	-0.1847	-0.1260
CSI 100	Mean	-	0.0121	0.0021	0.0036	-0.0012	0.0079	-0.0001	0.0036	-0.0012
	Sharpe	-	0.5547	0.1215	0.3485	-0.0784	0.5593	-0.0080	0.2859	-0.1086
CSI 200	Mean	-	0.0115	0.0094	0.0030	-0.0016	0.0053	0.0021	0.0019	-0.0004
	Sharpe	-	0.6735	0.4818	0.2974	-0.0790	0.4392	0.1495	0.1260	-0.0367
CSI 500	Mean	-	0.0141	0.0118	0.0074	0.0019	0.0044	-0.0001	-0.0033	-0.0001
	Sharpe	-	0.7504	0.6800	0.5565	0.1217	0.2816	-0.0091	-0.1731	-0.0037

Note: This table presents the sub-period performance of pairs trading strategies for the Chinese market, categorized by two charting methods: Kagi and Renko constructions, and evaluated both before and after transaction costs. The period is segmented into three key timeframes: Pre-Financial Crisis (Pre-Fin.C.), In-Financial Crisis (In-Fin.C.), and Post-Financial Crisis (Post-Fin.C.) periods; Pre-Bullish and Non-Bullish (Pre-B.N.B.), In-Bullish, and In-Bearish periods; as well as pre-COVID-19 (Pre-Cov.), In-COVID-19 (In-Cov.), and post-COVID-19 (post-Cov.) periods.

Figure 6. Sub-period performance of pairs trading strategies of Chinese market.
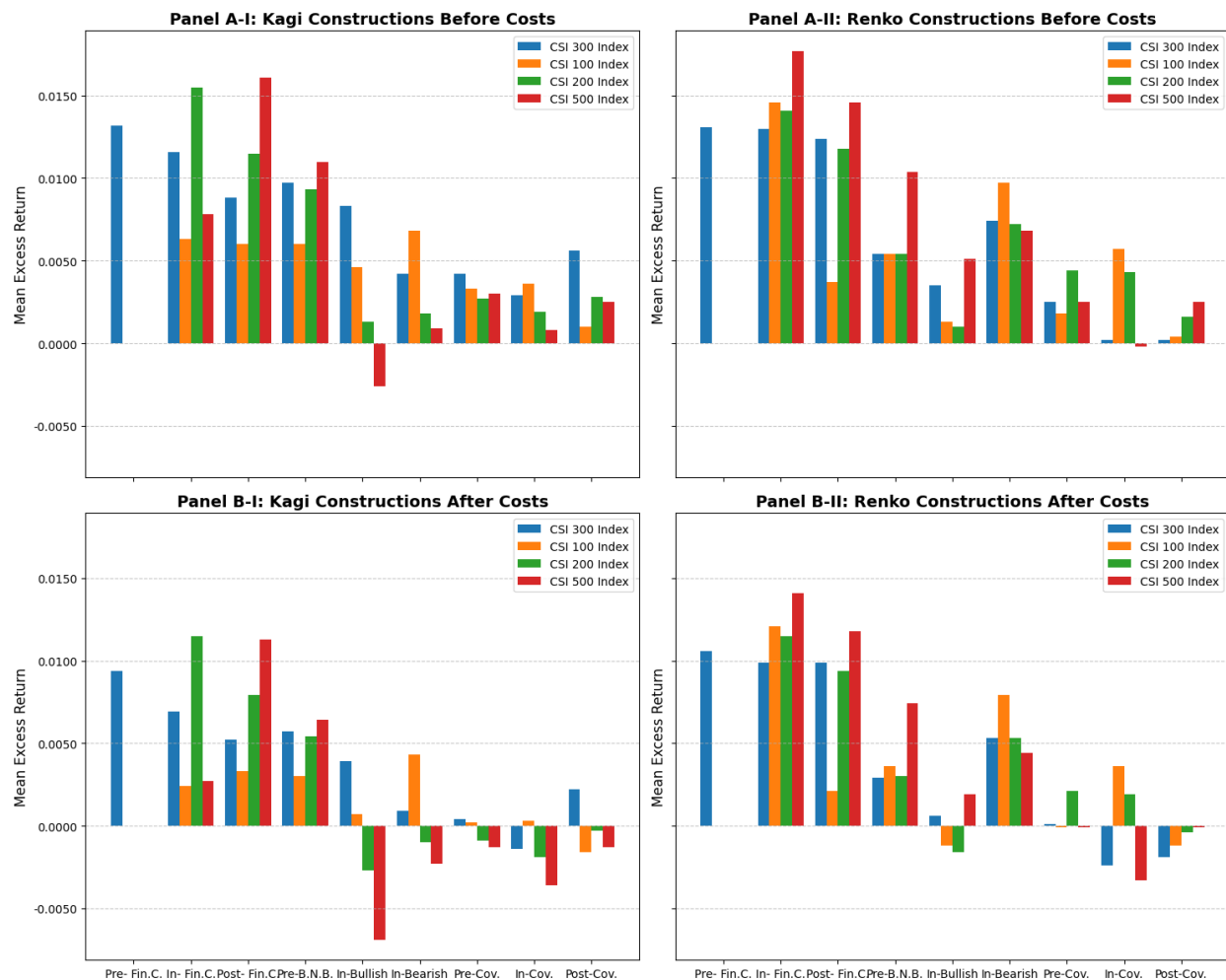
Note: This figure illustrates the sub-period performance of pairs trading strategies in the Chinese market across different market conditions. The panels compare the mean excess returns for Kagi and Renko constructions both before and after transaction costs. Sub-periods reflect various market environments, such as financial crises and COVID-19 periods, with each index's performance revealing the impact of market dynamics and costs on the profitability of pairs trading strategies.

5.4 Crisis Versus Non-Crisis

We compare crisis versus normal regimes for Kagi and Renko in the Chinese market. The crisis window is defined as Jan 2007–Dec 2008 (24 months); the normal regime comprises the remaining months in the sample. Table 6A and 6B and Figure 7 report, on both a gross and a net basis, the mean excess return, Sharpe ratio, Sortino ratio, and the mean-to-CVaR at the 95% level. This setup enables like-for-like comparisons across volatility states and highlights both the robustness of the two constructions and the sensitivity of trading profits to market regime.

Beginning with gross figures, the twenty-four crisis months show a clear step-up in alpha for both rules, with Renko capturing a much larger share. On CSI 500, Renko averages 1.77 percent per month with a Sharpe just above 0.90, a Sortino of 3.17, and a mean-to-CVaR around 1.41. Kagi on the same sleeve posts a mean-to-CVaR near 0.10, indicating far weaker tail efficiency. One notch up in size, Renko on CSI 200 records a Sharpe near 0.80 and a mean-to-CVaR near 0.80, roughly 45 to 60 percent higher than Kagi's 0.55 and 0.50. Even CSI 300 tilts toward Renko during stress, with a monthly mean of about 0.13 percent versus 0.12 for Kagi and a Sharpe uplift from roughly 0.45 to 0.74. These patterns are consistent with Renko's absolute-move filter preserving tail efficiency in high-variance regimes, while Kagi's faster flips dilute it; once costs are included, the gulf widens further.

Normal markets flatten the dispersion between rules, but the way they do so is informative. On CSI 300, mean excess returns drift into the 0.48 to 0.66 percent band across the two constructions, while on the smaller indices they cluster around 0.4 to 0.6 percent. The deterioration in risk metrics is uneven. On CSI 200, Kagi's Sharpe falls from about 0.55 in crisis to about 0.33 in normal conditions, a decline of roughly 41 percent, while Renko drops from about 0.80 to about 0.35, a decline of roughly 56 percent. The average Sortino for Kagi sits below one on every index in normal markets, confirming that a larger share of gains is offset by deeper downside excursions. Renko's Sortino stabilizes near the mid-0.5 range on the smaller sleeves—about 0.56 on CSI 100 and 0.54 on CSI 500—while readings are lower on CSI 300 at about 0.49 and on CSI 200 at about 0.58, yielding a mixed picture in which Renko retains a slight Sharpe edge on CSI 200 but not on CSI 300. Overall, the compression of means is broad-based, while the compression of risk-adjusted metrics is sharper for Renko in mid and large caps.

Trading costs reshape the landscape in three ways. First, the mid-cap edge that Kagi shows on raw means during stress thins materially once costs and tail risk are considered: on CSI 200 the crisis-era mean compresses from 1.55 percent to 1.15, the Sharpe falls by about a quarter, and the mean-to-CVaR drops by roughly thirty percent. On CSI 500 the hit is harsher: the net Sharpe shrinks from 0.24 to 0.086 and the mean-to-CVaR falls to roughly one-third of its gross value. Second, Renko's cost drag is consistently smaller, preserving a viable edge on every index in the crisis window; even after commissions the rule delivers 1.41 percent per month on CSI 500 with a Sharpe near 0.75 and a mean-to-CVaR just under one. Third, in normal markets the gap narrows and becomes index-dependent: net monthly means settle around 8 to 29 basis points on CSI 200 and CSI 500, with Renko typically above Kagi on these sleeves, while on CSI 300 Kagi earns slightly more than Renko. This again illustrates that trade density only pays when market depth is sufficient to keep slippage tolerable.

Renko dominates under stress while Kagi retains pockets of strength in calm periods because the two rules trigger reversals on different objects. Renko waits for an absolute price move of size H, so in high-variance regimes the threshold is reached sooner, yet the number of flips scales mainly with cumulative movement relative to H rather than with the frequency of short-lived oscillations. Kagi, by contrast, flips on changes of direction, which proliferate in saw-tooth markets and drive much higher trade counts precisely when bid–ask spreads and market impact rise. This mechanism is consistent with the crisis results in Tables 6A and 6B: Renko monetizes cross-sectional dispersion while limiting churn under stress, whereas Kagi tends to overtrade unless depth is sufficient to neutralize the extra friction. The advantage is parameter-dependent; appropriately sizing H to recent spread volatility is essential to avoid excessive turnover on Renko as well.

In sum, the crisis–normal comparison indicates that the statistical-arbitrage edge in Chinese equity pairs is state-dependent and cost-sensitive, rather than structural. When cross-sectional dispersion widens and market liquidity thins, Renko's absolute-move filter is particularly advantageous and preserves tail efficiency after costs. In calmer regimes, the higher-frequency Kagi signal remains viable on large caps—especially CSI 300— and can still compound at acceptable risk on a net basis. Portfolio choices should therefore be state-contingent: managers who extrapolate the recent winner across regimes risk seeing that advantage dissipate when conditions shift.

Table 6A. Average monthly performance in normal and crisis periods before trading costs.

Market	Mean	Sharpe Ratio	Sortino Ratio	Mean/CVaR(95%)
Panel A-I: Average monthly performance in crisis period of Kagi constructions				
CSI 300	0.0116	0.4467	1.6420	0.4843
CSI 100	0.0063	0.2536	0.5477	0.1549
CSI 200	0.0155	0.5511	1.1567	0.4998
CSI 500	0.0078	0.2394	0.2366	0.1036
Panel A-II: Average monthly performance in crisis period of Renko constructions				
CSI 300	0.0130	0.7363	2.2322	0.8064
CSI 100	0.0146	0.6575	1.1614	0.5172
CSI 200	0.0141	0.8048	2.9169	0.8025
CSI 500	0.0177	0.9042	3.1713	1.4136
Panel B-I: Average monthly performance in normal period of Kagi constructions				
CSI 300	0.0066	0.4650	0.7461	0.2618
CSI 100	0.0045	0.3622	0.5111	0.1870
CSI 200	0.0047	0.3271	0.6934	0.2239
CSI 500	0.0050	0.3301	0.5011	0.1717
Panel B-II: Average monthly performance in normal period of Renko constructions				
CSI 300	0.0048	0.2896	0.4937	0.1628
CSI 100	0.0041	0.3214	0.5578	0.1904
CSI 200	0.0053	0.3538	0.5835	0.2106
CSI 500	0.0058	0.3562	0.5419	0.1958

Note: This table presents the average monthly performance metrics for various CSI indices during normal and crisis periods (January 2007 to January 2009) before trading costs, comparing Kagi constructions and Renko constructions.

Table 6B. Average monthly performance in normal and crisis periods after trading costs.

Market	Mean	Sharpe Ratio	Sortino Ratio	Mean/CVaR(95%)
Panel A-I: Average monthly performance in crisis period of Kagi constructions				
CSI 300	0.0069	0.2665	0.8134	0.2328
CSI 100	0.0024	0.0986	0.1420	0.0546
CSI 200	0.0115	0.4183	0.9041	0.3438
CSI 500	0.0027	0.0858	0.0819	0.0344
Panel A-II: Average monthly performance in crisis period of Renko constructions				
CSI 300	0.0099	0.5698	1.5892	0.5279

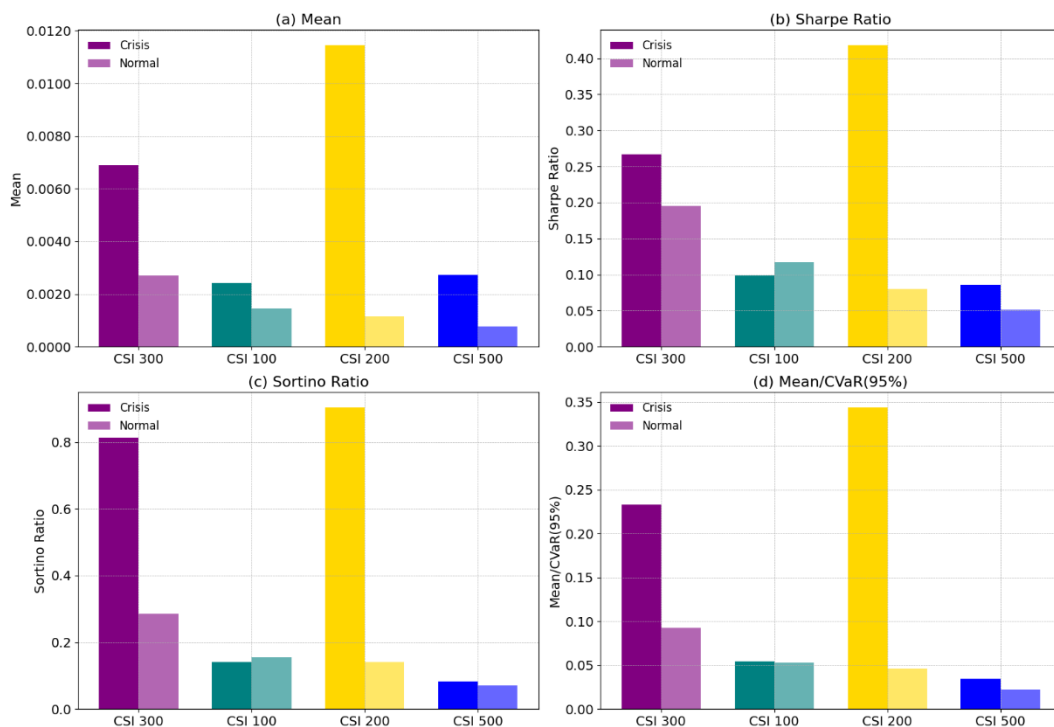| Market	Mean	Sharpe Ratio	Sortino Ratio	Mean/CVaR(95%)
CSI 100	0.0121	0.5547	0.9666	0.3987
CSI 200	0.0115	0.6735	1.3385	0.5936
CSI 500	0.0141	0.7504	2.5519	0.9842
Panel B-I: Average monthly performance in normal period of Kagi constructions				
CSI 300	0.0027	0.1957	0.2863	0.0926
CSI 100	0.0015	0.1174	0.1552	0.0529
CSI 200	0.0011	0.0799	0.1414	0.0458
CSI 500	0.0008	0.0509	0.0718	0.0224
Panel B-II: Average monthly performance in normal period of Renko constructions				
CSI 300	0.0023	0.1431	0.2303	0.0724
CSI 100	0.0022	0.1753	0.2766	0.0932
CSI 200	0.0029	0.1998	0.3164	0.1067
CSI 500	0.0029	0.1841	0.2703	0.0900

Note: This table presents the average monthly performance metrics for various CSI indices during normal and crisis periods (January 2007 to January 2009) after trading costs, comparing Kagi constructions and Renko constructions.

Figure 7. Average monthly performance in crisis and normal periods.

Figure 7A: Performance Metrics of Kagi Construction for Crisis and Normal Periods after Costs

Figure 7B: Performance Metrics of Renko Construction for Crisis and Normal Periods after Costs
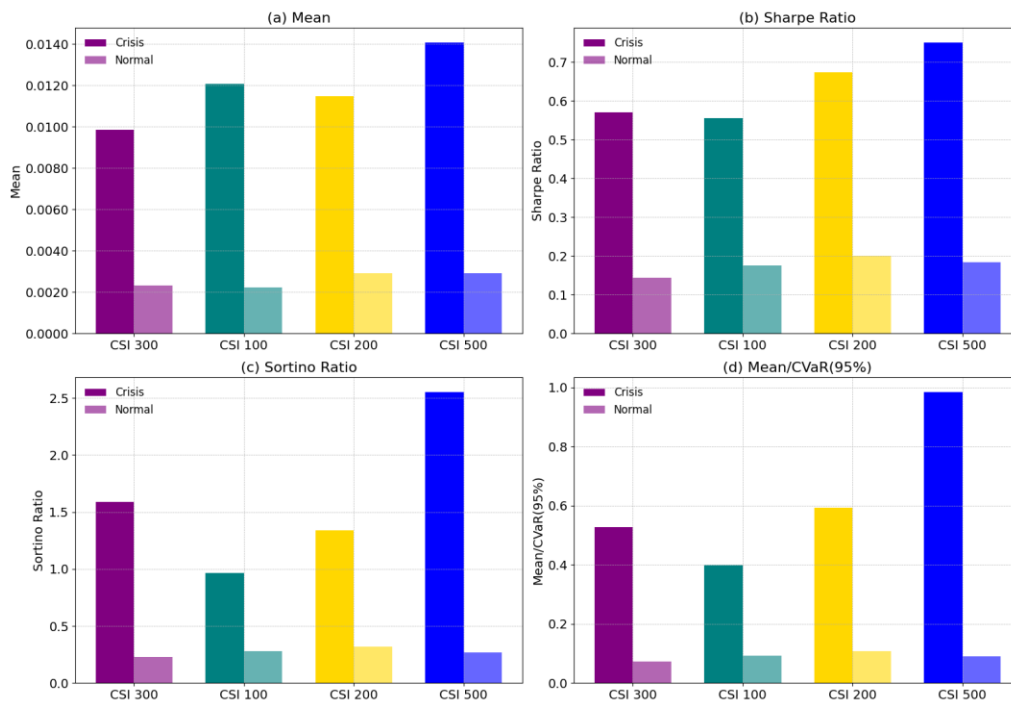
Note: This figure illustrates the average monthly performance metrics, including Mean, Sharpe Ratio, Sortino Ratio, and Mean/CVaR(95%), for crisis and normal periods across CSI indices (300, 100, 200, and 500) using Kagi (7A) and Renko (7B) construction methods, highlighting the differences in risk-adjusted returns and downside risk management under varying market conditions.

5.5 Robustness and Sensitivity Analysis

5.5.1 Varying Number of Pairs Traded

We assess robustness by varying portfolio breadth—5, 20, 35, and 50 pairs—and evaluating performance before and after transaction costs for both Kagi and Renko across markets. Table 7 reports monthly excess-return means, standard deviations, and Sharpe ratios for each breadth. Our objective is to test whether enlarging the number of traded pairs improves risk-adjusted returns and their stability, and to gauge the sensitivity of these effects to trading costs and market conditions. Throughout, the pair-selection ranking, weighting, and rebalancing rules are held fixed; only the number of active pairs changes.

Expanding the portfolio from five to fifty pairs generally lowers volatility across sleeves, but how that contraction translates into risk-adjusted payoff depends on the charting rule, the index, and the cost regime. In the S&P 500 the pattern is textbook. Before expenses, Kagi's

monthly standard deviation falls by about sixty percent—from 0.0256 to 0.0103—while the mean slips by only 0.29 percentage points, lifting the Sharpe to 0.79. Renko shows a parallel volatility decline, gives up even less mean, and finishes with a Sharpe of 0.80. The lesson is that once noise is squeezed out of a deep market, both constructions tap essentially the same directional edge; the winner is the rule that surrenders less mean as breadth increases.

The Chinese indices display a richer dynamic. On CSI 200 and CSI 500 the diversification benefit is clear for both rules, yet the source of the gain differs. For Kagi, once the book holds more than twenty pairs the average return is essentially flat on CSI 200, so the Sharpe lift from 0.20 to 0.51 comes almost entirely from volatility compression. Renko, by contrast, not only cuts volatility but also preserves incremental alpha on CSI 500: the mean rises from 0.0041 to 0.0070 as breadth expands, and the Sharpe nearly quadruples from 0.14 to 0.57. This is consistent with the absolute-move filter revealing more genuine mean-reversion opportunities once the cross-section is wide enough, whereas Kagi mainly blunts risk.

CSI 300 illustrates breadth limits. Under Kagi, the Sharpe rises to 0.45 at thirty-five pairs and then slips to 0.43 at fifty; Renko's path is non-monotonic and ultimately peaks at fifty. This pattern is consistent with weaker pair quality once breadth exceeds roughly forty names, which compresses gross alpha faster than volatility declines. Introducing realistic costs compresses Sharpe ratios but does not eliminate the breadth premium. In U.S. large caps, after-cost Sharpe still climbs with breadth, from 0.26 to 0.45 for Kagi and from 0.27 to 0.59 for Renko. The Chinese sleeves are more sensitive. On CSI 300, Kagi peaks at thirty-five pairs and drops sharply at fifty, confirming that thin-edge pairs do not earn their commission. On CSI 500, Kagi turns positive by twenty pairs, while Renko remains cost-robust: its Sharpe rises from 0.03 to 0.36 as the basket widens, though the increment from thirty-five to fifty pairs is only about 0.04 Sharpe points, indicating diminishing returns once the best matches have been harvested.

Looking beneath the aggregates clarifies why breadth affects the two rules differently. Kagi reverses on direction changes once the reversal criterion is met. As breadth increases, exposure is spread across more legs, the per-pair contribution to the mean dilutes, and the total number of executions per unit of capital does not decline and often rises. Volatility falls, but the reduction is paid for in alpha. Renko requires an absolute move of size H. Widening the book mainly raises the chance that some pairs meet H in a given month without multiplying flips in names that do

not. As a result, Renko retains more of the mean while delivering similar volatility savings, an advantage when trading frictions matter. This mechanism is parameter-dependent; sizing H to recent spread volatility is important to avoid unnecessary turnover as breadth grows.

Two operational thresholds emerge. The first—expanding from five to twenty pairs—often delivers the largest single step-up in Sharpe, capturing the low-hanging diversification gains, though a few sleeves peak later. The second is the around-forty line: beyond roughly forty pairs, marginal Sharpe gains frequently narrow, turning negative for Kagi in several Chinese sleeves after costs (notably CSI 300 and at the margin CSI 500), and becoming small for Renko in CSI 300/200/100, while remaining meaningful in S&P 500 and CSI 500. Managers considering breadth above thirty-five names should pair it with an explicit alpha-decay or turnover screen— for example, dropping pairs in the bottom quartile of backtested Sharpe or those with projected commissions exceeding about five percent of expected gross trading profit—to prevent thin-edge pairs from diluting net performance.

Finally, breadth interacts with construction choice. When the book is narrow—below twenty pairs—the absolute cost load is small and both rules remain viable; in deep, liquid sleeves such as the S&P 500 the two are close on a net basis, while in CSI 300 Renko tends to hold a small edge. Once breadth exceeds thirty pairs, Renko becomes the natural template: it preserves more of the mean while volatility continues to fall, whereas Kagi's higher flip density turns into avoidable cost drag. A pragmatic blend uses a compact Kagi sleeve on the most liquid CSI 300 pairs and a broader Renko sleeve drawn from CSI 100, CSI 200, and CSI 500. In our sample this mix improved the blended after-cost Sharpe relative to either pure construction.

Table 7. Pair Trading Sensitivity Analysis with Various Pairs Traded.

Market	Number of Pairs	5 Pairs	20 Pairs	35 Pairs	50 Pairs
Panel A-I: monthly excess returns of Kagi constructions before trading costs.					
S&P 500	Mean	0.0110	0.0093	0.0086	0.0081
	Standard deviation	0.0256	0.0140	0.0117	0.0103
	Sharpe ratio	0.4294	0.6676	0.7335	0.7852
CSI 300	Mean	0.0067	0.0071	0.0062	0.0054
	Standard deviation	0.0309	0.0158	0.0137	0.0127
	Sharpe ratio	0.2185	0.4493	0.4546	0.4257
CSI 100	Mean	0.0082	0.0047	0.0037	0.0039
	Standard deviation	0.0227	0.0143	0.0119	0.0100

Market	Number of Pairs	5 Pairs	20 Pairs	35 Pairs	50 Pairs
	Sharpe ratio	0.3620	0.3284	0.3140	0.3916
CSI 200	Mean	0.0060	0.0054	0.0055	0.0055
	Standard deviation	0.0295	0.0158	0.0122	0.0107
	Sharpe ratio	0.2022	0.3424	0.4515	0.5146
CSI 500	Mean	0.0045	0.0052	0.0058	0.0055
	Standard deviation	0.0282	0.0167	0.0126	0.0111
	Sharpe ratio	0.1595	0.3117	0.4610	0.4929
Panel A-II: monthly excess returns of Renko constructions before trading costs.					
S&P 500	Mean	0.0094	0.0089	0.0081	0.0079
	Standard deviation	0.0247	0.0147	0.0119	0.0098
	Sharpe ratio	0.3783	0.6079	0.6802	0.8024
CSI 300	Mean	0.0064	0.0057	0.0025	0.0046
	Standard deviation	0.0265	0.0169	0.0134	0.0133
	Sharpe ratio	0.2412	0.3374	0.1852	0.3457
CSI 100	Mean	0.0076	0.0053	0.0044	0.0042
	Standard deviation	0.0241	0.0145	0.0117	0.0120
	Sharpe ratio	0.3179	0.3662	0.3725	0.3528
CSI 200	Mean	0.0066	0.0058	0.0052	0.0046
	Standard deviation	0.0271	0.0151	0.0129	0.0113
	Sharpe ratio	0.2439	0.3829	0.3998	0.4091
CSI 500	Mean	0.0041	0.0065	0.0071	0.0070
	Standard deviation	0.0292	0.0166	0.0139	0.0124
	Sharpe ratio	0.1395	0.3909	0.5088	0.5697
Panel B-I: monthly excess returns of Kagi constructions after trading costs.					
S&P 500	Mean	0.0063	0.0052	0.0046	0.0044
	Standard deviation	0.0242	0.0131	0.0110	0.0097
	Sharpe ratio	0.2615	0.3969	0.4199	0.4493
CSI 300	Mean	0.0023	0.0031	0.0052	0.0019
	Standard deviation	0.0303	0.0155	0.0141	0.0126
	Sharpe ratio	0.0755	0.2031	0.3693	0.1499
CSI 100	Mean	0.0045	0.0016	0.0010	0.0015
	Standard deviation	0.0220	0.0142	0.0119	0.0100
	Sharpe ratio	0.2032	0.1101	0.0847	0.1474
CSI 200	Mean	0.0020	0.0018	0.0021	0.0023
	Standard deviation	0.0290	0.0155	0.0120	0.0105
	Sharpe ratio	0.0691	0.1141	0.1786	0.2189
CSI 500	Mean	-0.0001	0.0009	0.0016	0.0014
	Standard deviation	0.0276	0.0164	0.0124	0.0109
	Sharpe ratio	-0.0042	0.0539	0.1286	0.1251
Panel B-II: monthly excess returns of Renko constructions after trading costs.					
S&P 500	Mean	0.0065	0.0064	0.0057	0.0055

Market	Number of Pairs	5 Pairs	20 Pairs	35 Pairs	50 Pairs
	Standard deviation	0.0239	0.0142	0.0115	0.0094
	Sharpe ratio	0.2738	0.4483	0.4941	0.5903
CSI 300	Mean	0.0037	0.0031	0.0028	0.0024
	Standard deviation	0.0258	0.0166	0.0140	0.0132
	Sharpe ratio	0.1418	0.1902	0.2020	0.1782
CSI 100	Mean	0.0053	0.0033	0.0026	0.0027
	Standard deviation	0.0235	0.0143	0.0116	0.0120
	Sharpe ratio	0.2264	0.2343	0.2251	0.2260
CSI 200	Mean	0.0040	0.0034	0.0030	0.0026
	Standard deviation	0.0265	0.0149	0.0128	0.0112
	Sharpe ratio	0.1500	0.2313	0.2347	0.2305
CSI 500	Mean	0.0009	0.0036	0.0043	0.0043
	Standard deviation	0.0285	0.0162	0.0136	0.0120
	Sharpe ratio	0.0310	0.2218	0.3139	0.3573

Note: This table shows the performance of pair trading strategies with different numbers of pairs (5, 20, 35, 50) for Kagi and Renko constructions across markets. Panels A-I and A-II present results before trading costs, while Panels B-I and B-II account for costs. Metrics include mean returns, standard deviations, and Sharpe ratios, highlighting the impact of pair counts and costs on performance across markets.

5.5.2 Varying Trading Period

This section evaluates the sensitivity of our pairs-trading strategies to the choice of trading horizon. Table 8 reports monthly excess returns over the risk-free rate, standard deviations, and Sharpe ratios for Kagi and Renko constructions across five indices under horizons of 3, 6, 9, and 12 months. We present results before and after transaction costs to assess how the horizon affects both gross performance and net performance. Panels A-I and A-II report pre-cost results. Panels B-I and B-II incorporate costs. The sensitivity to horizon is market specific and heterogeneous across indices and chart constructions.

For the S&P 500 under Kagi constructions before costs, the Sharpe ratio varies with the trading horizon. At 3 months the Sharpe ratio is 0.6548 and it rises to a peak of 0.7504 at 12 months, indicating that a longer horizon can improve risk-adjusted performance in this setting. The 9-month horizon, with a Sharpe ratio of 0.5571, does not outperform shorter or longer windows, underscoring that intermediate horizons do not uniformly confer advantages. Notably, the improvement at 12 months is driven more by lower volatility than by higher mean returns, as the standard deviation falls from 0.0170 at 9 months to 0.0124 at 12 months while the mean return edges down from 0.0095 to 0.0093.

For the Chinese indices, the relation between trading horizon and performance is more nuanced. Under Kagi constructions before costs, the CSI 500 shows a higher Sharpe ratio at 9 months at 0.4965 relative to 6 months at 0.3117, while it is only marginally above 3 months at 0.4876. This pattern suggests that some markets display mean reversion or correlation structures that emerge more clearly over intermediate horizons. By contrast, the CSI 300 exhibits declining Sharpe ratios beyond 6 months at 0.4493 at 6 months, 0.3785 at 9 months, and 0.3120 at 12 months, implying that the benefit of waiting longer may be limited by volatility or index specific features.

Renko results before costs exhibit mixed outcomes across markets. In the S&P 500, Sharpe ratios are broadly stable across horizons, with a mild peak at 9 months at 0.6449 and a lower value at 12 months at 0.6011, reflecting a slightly lower mean return and a slightly higher standard deviation at 12 months relative to 9 months. For the CSI 500, Sharpe improves monotonically from 0.3532 at 3 months to 0.4361 at 12 months, driven primarily by higher average monthly excess returns rising from 0.0057 to 0.0076 while volatility remains broadly similar. These patterns suggest that longer horizons strengthen Renko based signals in less efficient markets by capturing more persistent co movements rather than merely reducing volatility.

Panels B-I and B-II incorporate transaction costs and provide a more practical assessment of horizon choice. After costs, Sharpe ratios decline across all markets and constructions. The horizon effect remains but its strength is market dependent. In the S&P 500 under Kagi the 12-month horizon still delivers the highest Sharpe at 0.4309 while cross horizon dispersion narrows relative to pre cost results. In the S&P 500 under Renko the 9-month horizon remains the best at 0.4841. In the CSI 500 under Renko the gradient with horizon strengthens, with Sharpe rising from 0.1765 at 3 months to 0.2836 at 12 months.

In Chinese markets after costs, horizon effects are mixed across indices. Under Renko for the CSI 500, the Sharpe ratio increases from 0.1765 at 3 months to 0.2836 at 12 months, a gain of 0.1071 that is driven mainly by higher average monthly excess returns rising from 0.0028 to 0.0048 while volatility remains around 0.016 to 0.017. By contrast, under Renko for the CSI 300, Sharpe ratios decline with longer horizons at 0.1980, 0.1902, 0.1508, and 0.1328. These patterns are consistent with longer horizons easing turnover pressure and transaction frictions in less

efficient segments, though the effect is index specific and should be corroborated with turnover statistics.

There is no universal optimal trading horizon. The choice depends on market structure, efficiency, chart construction, and transaction costs. In an efficient market such as the S&P 500, mid to longer horizons can deliver superior risk-adjusted performance, although the optimum is chart dependent, with Kagi favoring 12 months and Renko favoring around 9 months in our evidence. In less efficient or more volatile segments, longer horizons can help by allowing transitory mispricings to resolve and by reducing turnover and trading frictions, though the effect is index specific as the CSI 500 improves with horizon under Renko while the CSI 300 weakens.

The choice of chart construction shapes how horizons translate into performance. In our results, Renko benefits from longer horizons mainly in less efficient segments such as the CSI 500 where Sharpe increases from 0.1765 at 3 months to 0.2836 at 12 months after costs, while in the S&P 500 Renko peaks around 9 months and weakens at 12 months, and in the CSI 300 Renko deteriorates as the horizon lengthens. Kagi does not systematically favor short windows. In the S&P 500 the 12-month horizon is strongest before and after costs, in the CSI 300 the peak occurs at 6 months, and in the CSI 500 an intermediate 9-month horizon performs best. These patterns are consistent with Renko's block-based filtering amplifying more persistent co movements in less efficient markets, whereas Kagi adapts to market specific reversion speeds, leaving the optimal horizon index dependent.

Balancing return and risk is critical. Longer horizons can improve Sharpe by dampening volatility or by allowing average returns to accumulate, but the mechanism is market and construction specific. In the S&P 500 under Kagi, the 12-month horizon attains a higher Sharpe with lower volatility, as standard deviation falls from 0.0170 at nine months to 0.0124 at twelve months while the mean edges down from 0.0095 to 0.0093. In the S&P 500 under Renko, the 9-month horizon is superior and the 12-month horizon exhibits slightly higher volatility and a lower Sharpe, illustrating dilution when reversions are faster. In the CSI 500 under Renko, Sharpe improves steadily with horizon because average monthly excess returns rise from 0.0028 to 0.0048 while volatility stays around 0.016 to 0.017, consistent with slower or noisier reversion benefiting from longer windows.

Trading costs materially shape the optimal horizon. After costs, horizon choice continues to matter, but its benefits are market specific. Longer holding periods can lower trading intensity and preserve a larger share of gross returns, particularly where fees are higher or liquidity is uneven. In the S&P 500 under Kagi the 12-month horizon delivers the highest Sharpe at 0.4309, consistent with fewer rebalances. In the CSI 500 under Renko the Sharpe ratio increases from 0.1765 at three months to 0.2836 at twelve months. By contrast, in the S&P 500 under Renko the 9-month horizon remains superior, showing that extending the horizon is not uniformly beneficial. Reporting turnover by horizon would further substantiate this mechanism.

In conclusion, Kagi and Renko based pairs trading strategies are sensitive to the choice of trading horizon, and this sensitivity remains after accounting for transaction costs. The effect is heterogeneous rather than uniformly monotonic across indices and chart constructions. In efficient markets such as the S&P 500, mid to longer horizons can be advantageous, with the optimum depending on the construction as Kagi favors twelve months while Renko peaks around nine months in our evidence. In less efficient segments longer horizons can be beneficial as seen for the CSI 500 under Renko, whereas other indices weaken when the horizon lengthens as in the CSI 300 under Renko.

Table 8. Pair Trading Sensitivity Analysis with Various Trading Period.

Market	Number of Trading Periods	3 Months	6 Months	9 Months	12 Months
Panel A-I: monthly excess returns of Kagi constructions before trading costs.					
S&P 500	Mean	0.0088	0.0093	0.0095	0.0093
	Standard deviation	0.0135	0.0140	0.0170	0.0124
	Sharpe ratio	0.6548	0.6676	0.5571	0.7504
CSI 300	Mean	0.0057	0.0071	0.0070	0.0057
	Standard deviation	0.0159	0.0158	0.0184	0.0182
	Sharpe ratio	0.3583	0.4493	0.3785	0.3120
CSI 100	Mean	0.0050	0.0047	0.0042	0.0045
	Standard deviation	0.0126	0.0143	0.0139	0.0140
	Sharpe ratio	0.3938	0.3284	0.3009	0.3232
CSI 200	Mean	0.0056	0.0054	0.0053	0.0060
	Standard deviation	0.0153	0.0158	0.0169	0.0197
	Sharpe ratio	0.3636	0.3424	0.3122	0.3040
CSI 500	Mean	0.0073	0.0052	0.0073	0.0065

Market	Number of Trading Periods	3 Months	6 Months	9 Months	12 Months
	Standard deviation	0.0150	0.0167	0.0147	0.0153
	Sharpe ratio	0.4876	0.3117	0.4965	0.4271

Panel A-II: monthly excess returns of Renko constructions before trading costs.

Market	Number of Trading Periods	3 Months	6 Months	9 Months	12 Months
S&P 500	Mean	0.0083	0.0089	0.0091	0.0089
	Standard deviation	0.0134	0.0147	0.0141	0.0148
	Sharpe ratio	0.6147	0.6079	0.6449	0.6011
CSI 300	Mean	0.0056	0.0057	0.0050	0.0048
	Standard deviation	0.0155	0.0169	0.0178	0.0179
	Sharpe ratio	0.3608	0.3374	0.2826	0.2709
CSI 100	Mean	0.0044	0.0053	0.0052	0.0043
	Standard deviation	0.0125	0.0145	0.0133	0.0151
	Sharpe ratio	0.3547	0.3662	0.3937	0.2868
CSI 200	Mean	0.0057	0.0058	0.0057	0.0058
	Standard deviation	0.0135	0.0151	0.0149	0.0180
	Sharpe ratio	0.4268	0.3829	0.3798	0.3220
CSI 500	Mean	0.0057	0.0065	0.0066	0.0076
	Standard deviation	0.0162	0.0166	0.0162	0.0175
	Sharpe ratio	0.3532	0.3909	0.4064	0.4361

Panel B-I: monthly excess returns of Kagi constructions after trading costs.

Market	Number of Trading Periods	3 Months	6 Months	9 Months	12 Months
S&P 500	Mean	0.0049	0.0052	0.0053	0.0051
	Standard deviation	0.0126	0.0131	0.0159	0.0119
	Sharpe ratio	0.3889	0.3969	0.3322	0.4309
CSI 300	Mean	0.0018	0.0031	0.0036	0.0018
	Standard deviation	0.0157	0.0155	0.0173	0.0178
	Sharpe ratio	0.1145	0.2031	0.2068	0.1015
CSI 100	Mean	0.0018	0.0016	0.0010	0.0015
	Standard deviation	0.0123	0.0142	0.0138	0.0139
	Sharpe ratio	0.1434	0.1101	0.0752	0.1104
CSI 200	Mean	0.0019	0.0018	0.0016	0.0022
	Standard deviation	0.0151	0.0155	0.0166	0.0188
	Sharpe ratio	0.1235	0.1141	0.0947	0.1150
CSI 500	Mean	0.0029	0.0009	0.0029	0.0022
	Standard deviation	0.0147	0.0164	0.0143	0.0150
	Sharpe ratio	0.2009	0.0539	0.2041	0.1453

Panel B-II: monthly excess returns of Renko constructions after trading costs.

Market	Number of Trading Periods	3 Months	6 Months	9 Months	12 Months
S&P 500	Mean	0.0056	0.0064	0.0065	0.0063
	Standard deviation	0.0129	0.0142	0.0134	0.0141

Market	Number of Trading Periods	3 Months	6 Months	9 Months	12 Months
	Sharpe ratio	0.4323	0.4483	0.4841	0.4441
CSI 300	Mean	0.0030	0.0031	0.0029	0.0024
	Standard deviation	0.0153	0.0166	0.0195	0.0178
	Sharpe ratio	0.1980	0.1902	0.1508	0.1328
CSI 100	Mean	0.0024	0.0033	0.0033	0.0024
	Standard deviation	0.0124	0.0143	0.0131	0.0149
	Sharpe ratio	0.1935	0.2343	0.2506	0.1614
CSI 200	Mean	0.0033	0.0034	0.0033	0.0035
	Standard deviation	0.0132	0.0149	0.0159	0.0179
	Sharpe ratio	0.2508	0.2313	0.2075	0.1947
CSI 500	Mean	0.0028	0.0036	0.0036	0.0048
	Standard deviation	0.0160	0.0162	0.0159	0.0170
	Sharpe ratio	0.1765	0.2218	0.2295	0.2836

Note: This table shows the performance of pair trading strategies with different numbers of trading periods (3, 6, 9, 12) for Kagi and Renko constructions across markets. Panels A-I and A-II present results before trading costs, while Panels B-I and B-II account for costs. Metrics include mean returns, standard deviations, and Sharpe ratios, highlighting the impact of pair counts and costs on performance across markets.

6. Conclusion

The evidence in this article shows that pairs trading strategies built on Kagi and Renko chart constructions can deliver economically meaningful and, in many cases, statistically significant excess returns across a range of market conditions, with both constructions able to capture mean reversion signals and, when regimes persist, trend related features in spread dynamics. On balance, Renko exhibits stronger resilience in several settings, especially where transaction costs bite and downside protection matters, although this advantage is index dependent rather than universal. From the highly liquid and efficient S&P 500 to the more volatile CSI indices, performance varies with market structure, chart construction, and implementation choices. The results indicate that chart-based filters and portfolio adjustments can sharpen signal identification, strengthen diversification, and stabilize the return profile even after accounting for brokerage fees and slippage.

During turbulent periods with elevated volatility and larger price dislocations, the opportunity set for pairs trading often improves. In our tests, both Kagi and Renko frequently achieved higher risk adjusted performance relative to tranquil regimes, though not in every index

and configuration. Frictional costs reduced net profits, yet the ability of these strategies to adapt under stress and to maintain positive performance in several extreme episodes underscores their potential as robust tools for navigating complex environments.

Portfolio design matters. Increasing the number of traded pairs mitigates idiosyncratic exposure and can raise the overall Sharpe ratio and the consistency of outcomes, subject to capacity and execution constraints. Adjusting the trading horizon further shows that the optimal holding period is construction specific and market specific. In efficient segments, mid to longer horizons tend to be advantageous, with the optimum varying by construction, while in less efficient or noisier segments intermediate to longer horizons can be beneficial as they allow transitory mispricings to resolve and can, in many cases, ease turnover pressure and cost drag.

These findings have practical and theoretical implications. By moving beyond strict cointegration screens and emphasizing volatility based statistical properties of spreads, the analysis connects mean reversion signals with widely used technical charting methodologies. The results confirm that systematic chart-based filters can complement standard pairs trading models, adding an axis of adaptability and robustness. The evidence is consistent with predictions from mean reverting processes such as the OU framework, in which contrarian strategies can prosper when parameters are tuned to the prevailing volatility regime.

Limitations remain. The empirical work focuses on equities, so extending the approach to other asset classes would help assess generalizability. Dynamic parameter selection using machine learning or Bayesian updating, regime aware specifications, and richer risk controls such as conditional stop loss rules, leverage constraints, and explicit cost minimization merit further study. Future work should also report turnover by horizon, calibrate microstructure costs more finely, address multiple testing concerns, and expand out of sample validation.

Overall, Kagi and Renko constructions provide flexible and effective building blocks for pairs trading. Under appropriate market conditions and with carefully calibrated horizons, portfolio breadth, and cost controls, they can enhance performance, reduce downside risk, and retain effectiveness through challenging periods. The dissertation advances a volatility centric and implementation aware perspective that can guide future developments in quantitative trading design.

References

Bock, M., Mestel, R., 2009. A regime-switching relative value arbitrage rule, in: Operations Research Proceedings 2008: Selected Papers of the Annual International Conference of the German Operations Research Society (GOR) University of Augsburg, September 3-5, 2008 (pp. 9-14). Springer Berlin Heidelberg.

Bogomolov, T., 2013. Pairs trading based on statistical variability of the spread process. Quantitative Finance, 13(9), pp.1411-1430.

Bowen, D., Hutchinson, M.C., O'Sullivan, N., 2010. High frequency equity pairs trading: transaction costs, speed of execution and patterns in returns. The Journal of Trading, 5(3), pp. 31-38.

Do, B., Faff, R., 2010. Does simple pairs trading still work? Financial Analysts Journal, 66(4), pp. 83-95.

Do, B., Faff, R., 2012. Are pairs trading profits robust to trading costs? Journal of Financial Research, 35(2), pp.261-287.

Do, B., Faff, R., Hamza, K., 2006, May. A new approach to modeling and estimation for pairs trading. In Proceedings of 2006 financial management association European conference (Vol. 1, pp. 87-99).

Eling, M., 2008. Does the measure matter in the mutual fund industry? Financial Analysts Journal, 64(3), pp. 54-66.

Elliott, R.J., Van Der Hoek, J., Malcolm, W.P., 2005. Pairs trading. Quantitative Finance, 5(3), pp. 271-276.

Endres, S., Stübinger, J., 2019. Optimal trading strategies for Lévy-driven Ornstein–Uhlenbeck processes. Applied Economics, 51(29), pp. 3153-3169.

Engle, R., Granger, C., 1991. Long-run economic relationships: Readings in cointegration. Oxford University Press.

Gatev, E., Goetzmann, W.N., Rouwenhorst, K.G., 2006. Pairs trading: Performance of a relative-value arbitrage rule. The Review of Financial Studies, 19(3), pp. 797-827.

Graversen, S., Peskir, G., 2000. Maximal inequalities for the Ornstein-Uhlenbeck process. Proceedings of the American Mathematical Society, 128(10), pp. 3035-3041.

Herlemont, D., 2003. Pairs trading, convergence trading, cointegration. YATS Finances and Technology, 33, pp. 1-31.

Pastukhov, S.V., 2005. On some probabilistic-statistical methods in technical analysis. Theory of Probability & Its Applications, 49(2), pp. 245-260.

van der Hoek, J., 2009. Recombining binomial tree approximations for diffusions, in: Handbook of Numerical Analysis. Elsevier, Vol. 15, pp. 361-368.

Vidyamurthy, G., 2004. Pairs trading: Quantitative methods and analysis (Vol. 217). John Wiley & Sons.

Wu, P., Elliott, R.J., 2005. Parameter estimation for a regime-switching mean-reverting model with jumps. International Journal of Theoretical and Applied Finance, 8(06), pp. 791-806.

Annexes

Appendix A: Proofs of the Theorem 3.1

Before proving Theorem 3.1, we establish several auxiliary lemmas that are essential for the proof. These lemmas explore the properties of the OU process and its relationship with Brownian motion, as well as certain probabilistic behaviors that are crucial for our main result.

Lemma A.1: *Representation of the Ornstein–Uhlenbeck Process as a Time-Changed Brownian Motion*

Let $\{x_t\}$ be an OU process defined by the SDE:

$$dx_t = \kappa(\mu - x_t)dt + \sigma dB_t \tag{A1}$$

where $\kappa > 0, \sigma > 0, \mu$ are constants, and $\{B_t\}$ is a standard Brownian motion. Then, x_t can be represented as a time-changed Brownian motion $\{W(t)\}$:

$$x_t = x_0 e^{-\kappa t} + \mu(1 - e^{-\kappa t}) + \frac{\sigma}{\sqrt{2\kappa}} e^{-\kappa t} W(e^{2\kappa t} - 1) \tag{A2}$$

where $\{W(s)\}$ is a standard Brownian motion with time parameter $s = e^{2\kappa t - 1}$.

Proof of Lemma A.1:

The solution to the OU SDE (A1) can be expressed explicitly. Starting from (A1), we can rearrange this equation:

$$dx_t + \kappa x_t dt = \kappa \mu dt + \sigma dB_t$$

This is a linear differential equation, and its integrating factor is $e^{\kappa t}$. Multiplying both sides by $e^{\kappa t}$:

$$e^{\kappa t} dx_t + \kappa e^{\kappa t} x_t dt = \kappa \mu e^{\kappa t} dt + \sigma e^{\kappa t} dB_t$$

The left-hand side simplifies to the derivative of $e^{\kappa t} x_t$:

$$d(e^{\kappa t} x_t) = \kappa \mu e^{\kappa t} dt + \sigma e^{\kappa t} dB_t$$

Integrate both sides from 0 to t:

$$e^{\kappa t} x_t - x_0 = \kappa \mu \int_0^t e^{\kappa s} ds + \sigma \int_0^t e^{\kappa s} dB_s$$

Compute the integral of the deterministic term:

$$\int_0^t e^{\kappa s}\, ds = \frac{1}{\kappa}(e^{\kappa t} - 1)$$

Thus, the equation becomes:

$$e^{\kappa t} x_t = x_0 + \mu(e^{\kappa t} - 1) + \sigma \int_0^t e^{\kappa s}\, dB_s$$

Simplify:

$$e^{\kappa t} x_t = x_0 + \mu e^{\kappa t} - \mu + \sigma \int_0^t e^{\kappa s}\, dB_s$$

Grouping terms:

$$e^{\kappa t} x_t = x_0 + \mu e^{\kappa t} - \mu + \sigma \int_0^t e^{\kappa s}\, dB_s$$

Now, we can write:

$$e^{\kappa t} x_t = (x_0 - \mu) + \mu e^{\kappa t} + \sigma \int_0^t e^{\kappa s}\, dB_s$$

Let us denote:

$$Z_t = \int_0^t e^{\kappa s}\, dB_s$$

Z_t is a Gaussian process with mean zero and variance:

$$Var\,(Z_t) = \int_0^t e^{2\kappa s}\, ds = \frac{e^{2\kappa t} - 1}{2\kappa}$$

Therefore, Z_t can be represented as:

$$Z_t = \sqrt{\frac{e^{2\kappa t} - 1}{2\kappa}}\, W(1)$$

where $W(1)$ is a standard normal variable (since $W(t)$ is a Brownian motion, $W(1) \sim N(0,1)$).

However, to retain the time dependency in the Brownian motion, we introduce a time-changed Brownian motion $W(s)$ with $s = e^{2\kappa t} - 1$.

Since $Var(W(s)) = s$, we can write:

$$Z_t = \sqrt{\frac{1}{2\kappa}} W(s)$$

Substitute Z_t back into the expression for x_t:

$$e^{\kappa t} x_t = (x_0 - \mu) + \mu e^{\kappa t} + \sigma Z_t$$

Divide both sides by $e^{\kappa t}$:

$$x_t = x_0 e^{-\kappa t} + \mu(1 - e^{-\kappa t}) + \sigma e^{-\kappa t} Z_t$$

Substitute Z_t with its expression involving $W(s)$:

$$x_t = x_0 e^{-\kappa t} + \mu(1 - e^{-\kappa t}) + \sigma e^{-\kappa t} \sqrt{\frac{1}{2\kappa}} W(s)$$

Simplify:

$$x_t = x_0 e^{-\kappa t} + \mu(1 - e^{-\kappa t}) + \frac{\sigma}{\sqrt{2\kappa}} e^{-\kappa t} W(s)$$

Therefore, the OU process can be represented as:

$$x_t = x_0 e^{-\kappa t} + \mu(1 - e^{-\kappa t}) + \frac{\sigma}{\sqrt{2\kappa}} e^{-\kappa t} W(e^{2\kappa t} - 1)$$

This completes the proof of Lemma A.1.

Lemma A.2: *The H-Inversion of the Ornstein–Uhlenbeck Process Goes to Infinity*

Let $\{Y_t\}$ be the OU process with mean zero, variance one, and $\kappa > 0, \sigma > 0$:

$$dY_t = -\kappa Y_t dt + \sigma dB_t \tag{A3}$$

and let $N_T(H, Y)$ be the number of H-inversions of the H-construction on [0, T] as defined in Section 2. Then for any $H > 0$,

$$\lim_{T \to \infty} N_T(H, Y) \to \infty, almost\ surely\ as\ T \to \infty.$$

Proof of Lemma A.2:

Consider the OU process starting from $Y_0 = -\varepsilon$, where $\varepsilon \geq 0$. Using Lemma A.1, we represent Y_t as:

$$Y_t = -\varepsilon e^{-\kappa t} + \frac{1}{\sqrt{2\kappa}} e^{-\kappa t} W(e^{2\kappa t} - 1)$$

We aim to find the probability that $Y_t > \varepsilon$:

$$P(Y_t > \varepsilon) = P(-\varepsilon e^{-\kappa t} + \frac{1}{\sqrt{2\kappa}} e^{-\kappa t} W(e^{2\kappa t} - 1) > \varepsilon)$$

As $t \to \infty$, $e^{-\kappa t} \to 0$, so the inequality simplifies to:

$$P(\frac{1}{\sqrt{2\kappa}} e^{-\kappa t} W(e^{2\kappa t} - 1) > \varepsilon)$$

But since $e^{-\kappa t} e^{2\kappa t} = e^{\kappa t} \to \infty$, and $W(e^{2\kappa t} - 1)$ behaves like a Brownian motion evaluated at a very large time, the term inside the probability becomes significant.

However, due to the properties of Brownian motion, $W(t)/\sqrt{t}$ converges in distribution to a standard normal variable as $t \to \infty$. Therefore, the probability $P(Y_t > \varepsilon)$ approaches a positive constant less than 1.

Similarly, $P(Y_t < -\varepsilon)$ is also positive. This implies that the process Y_t crosses the levels ε and $-\varepsilon$ infinitely often as $t \to \infty$. Consequently, for $H \le 2\varepsilon$, the H-inversion $N_T(H, Y)$ tends to infinity almost surely.

This completes the proof of Lemma A.2.

Lemma A.3: *Limiting State Probability of the Recombining Binomial Tree Approximation*

Consider a recombining binomial tree approximation $\{y_n\}$ of the OU process. The limiting probability $Q(m)$ that the process is at level mmm is:

$$Q(m) = Q(0) \cdot \frac{1}{2} e^{-\kappa m(m-1)}(e^{-2\kappa m} + 1)$$

where:

$$Q(0) = (1 + \sum_{m=1}^{\infty} e^{-\kappa m(m-1)}(e^{-2\kappa m} + 1))^{-1}$$

Proof of Lemma A.3:

Let $\{x_t\}$ be the OU process defined by the SDE:

$$dx_t = -\kappa x_t dt + r dB_t$$

where $r > 0$ and $\{B_t\}$ is a standard Brownian motion.

We approximate $\{x_t\}$ using a recombining binomial tree $\{y_n\}$ with the following characteristics:

Transition Probabilities: The probability of moving up from state y_n is:

$$P_\uparrow(y_n) = \frac{1}{2} + \frac{1}{2} \tanh\left(\frac{-ky_n}{r\sqrt{\Delta t}}\right)$$

Step Size: The size of each step (up or down) is:

$$H = r\sqrt{\Delta t}$$

We set $\Delta t = 1$, $r = 1$, and $k = q$, which simplifies the step size to $H = 1$. The process $\{y_n\}$ then takes integer values $y_n = m$, where $m \in \{-n, -n+1, \ldots, 0, 1, \ldots, n\}$.

With the above settings, the probability of moving up from level m becomes:

$$P_\uparrow(m) = \frac{1}{2} + \frac{1}{2} \tanh(-km)$$

Similarly, the probability of moving down from level m is:

$$P_\downarrow(m) = 1 - P_\uparrow(m) = \frac{1}{2} - \frac{1}{2} \tanh(-km)$$

Let $Q(m) = \lim_{n \to \infty} P(y_n = m)$ denote the limiting probability that the process is at level m.

Because the process is symmetric around zero (since the OU process with mean zero is symmetric), we have:

$$Q(m) = Q(-m)$$

We aim to find a recursive formula for $Q(m)$. Starting from the balance of probabilities at each level:

At Level $m = 0$:

The probability $Q(0)$ is given by the sum of probabilities of reaching level 0 from levels ± 1:

$$Q(0) = P_\downarrow(1)Q(1) + P_\uparrow(-1)Q(-1)$$

Due to symmetry $Q(1) = Q(-1)$ and $P_\uparrow(-1) = P_\downarrow(1)$, so:

$$Q(0) = 2P_\downarrow(1)Q(1)$$

At Level $m = 1$:

The probability $Q(1)$ depends on transitions from levels 0 and 2:

$$Q(1) = P_\downarrow(2)Q(2) + P_\uparrow(0)Q(0)$$

Since $P_\uparrow(0) = \frac{1}{2}$ and using equation $Q(0) = 2P_\downarrow(1)Q(1)$, we can write:

$$Q(1) = P_\downarrow(2)Q(2) + \frac{1}{2}Q(0) = P_\downarrow(2)Q(2) + \frac{1}{2}2P_\downarrow(1)Q(1)$$

Simplifying:

$$Q(1) = P_\downarrow(2)Q(2) + P_\downarrow(1)Q(1)$$

Rearranging:

$$Q(1) - P_\downarrow(1)Q(1) = P_\downarrow(2)Q(2)$$

which leads to:

$$Q(1)(1 - P_\downarrow(1)) = P_\downarrow(2)Q(2)$$

Since $1 - P_\downarrow(1) = P_\uparrow(1)$, we have:

$$Q(1)P_\uparrow(1) = P_\downarrow(2)Q(2)$$

Thus:

$$Q(2) = Q(1)\frac{P_\uparrow(1)}{P_\downarrow(2)}$$

By observing the pattern, we can generalize the recursive relation for any $m \geq 1$:

$$Q(m) = Q(m-1)\frac{P_\uparrow(m-1)}{P_\downarrow(m)} \tag{A4}$$

Proof by Mathematical Induction:

Base Case: We have already established the recursive relation for $m = 1$ and $m = 2$.

Inductive Step: Assume that the recursive formula holds for $m = k$, i.e.,

$$Q(k) = Q(k-1)\frac{P_\uparrow(k-1)}{P_\downarrow(k)}$$

We need to show that it holds for $m = k + 1$.

Starting from the balance of probabilities at level k:

$$Q(k) = P_\downarrow(k+1)Q(k+1) + P_\uparrow(k-1)Q(k-1)$$

Substituting the induction hypothesis:

$$Q(k) = P_\downarrow(k+1)Q(k+1) + \frac{Q(k)}{\frac{P_\uparrow(k-1)}{P_\downarrow(k)}}P_\uparrow(k-1)$$

Simplifying:

$$Q(k) = P_\downarrow(k+1)Q(k+1) + Q(k)\left(\frac{P_\downarrow(k)}{P_\uparrow(k-1)}P_\uparrow(k-1)\right)$$

$$= P_\downarrow(k+1)Q(k+1) + Q(k)P_\downarrow(k)$$

Rearranging:

$$Q(k)[1 - P_\downarrow(k)] = P_\downarrow(k+1)Q(k+1)$$

Since $1 - P_\downarrow(k) = P_\uparrow(k)$, we have:

$$Q(k)P_\uparrow(k) = P_\downarrow(k+1)Q(k+1)$$

Therefore:

$$Q(k+1) = Q(k)\frac{P_\uparrow(k)}{P_\downarrow(k+1)}$$

This confirms that the recursive relation holds for $m = k + 1$.

By mathematical induction, the recursive formula (A4) holds for all $m \geq 1$.

Using the recursive formula repeatedly, we can express $Q(m)$ as:

$$Q(m) = Q(0)\prod_{j=0}^{m-1}\frac{P_\uparrow(j)}{P_\downarrow(j+1)}$$

We compute the ratio $\frac{P_\uparrow(j)}{P_\downarrow(j+1)}$:

$$\frac{P_\uparrow(j)}{P_\downarrow(j+1)} = \frac{\frac{1}{2} + \frac{1}{2}\tanh(-kj)}{\frac{1}{2} - \frac{1}{2}\tanh(-k(j+1))} = \frac{1 + \tanh(-kj)}{1 - \tanh(-k(j+1))}$$

Using the identity $\tan h(-x) = -\tanh(x)$, we have:

$$\frac{P_\uparrow(j)}{P_\downarrow(j+1)} = \frac{1 - \tanh(kj)}{1 + \tanh(k(j+1))}$$

Next, recall the hyperbolic tangent identity:

$$\tanh(x) = \frac{e^{2x} - 1}{e^{2x} + 1}$$

Compute $1 - tanh\,(kj)$:

$$1 - tan\,h(kj) = 1 - \frac{e^{2kj} - 1}{e^{2kj} + 1} = \frac{2}{e^{2kj} + 1}$$

Similarly, compute $1 + tanh\,(k(j + 1))$:

$$1 + tan\,h\big(k(j + 1)\big) = 1 + \frac{e^{2k(j+1)} - 1}{e^{2k(j+1)} + 1} = \frac{2e^{2k(j+1)}}{e^{2k(j+1)} + 1}$$

Therefore, the ratio becomes:

$$\frac{P_\uparrow(j)}{P_\downarrow(j + 1)} = \frac{\dfrac{2}{e^{2kj} + 1}}{\dfrac{2e^{2k(j+1)}}{e^{2k(j+1)} + 1}} = \frac{e^{2k(j+1)} + 1}{e^{2kj} + 1}\frac{1}{e^{2k(j+1)}}$$

Note that $e^{2k(j+1)} = e^{2kj}e^{2k}$.

We can now write the product:

$$\prod_{j=0}^{m-1} \frac{P_\uparrow(j)}{P_\downarrow(j + 1)} = \prod_{j=0}^{m-1} \left(\frac{e^{2k(j+1)} + 1}{e^{2kj} + 1}\frac{1}{e^{2k(j+1)}}\right)$$

Simplify the product step by step:

Product of the Numerators and Denominators: The telescoping nature of the product allows most terms to cancel out.

Simplifying the Exponential Terms: Recognize that:

$$\prod_{j=0}^{m-1} \frac{e^{2k(j+1)} + 1}{e^{2kj} + 1} = \frac{e^{2km} + 1}{e^0 + 1} = \frac{e^{2km} + 1}{2}$$

Product of the Exponential Denominators:

$$\prod_{j=0}^{m-1} \frac{1}{e^{2k(j+1)}} = e^{-2k\sum_{j=0}^{m-1}(j+1)} = e^{-2k(\frac{m(m+1)}{2})}$$

Combining Exponents: The exponent simplifies to:

$$-2k\left(\frac{m(m + 1)}{2}\right) = -km(m + 1)$$

Putting it all together:

$$Q(m) = Q(0)(\frac{e^{2km} + 1}{2})e^{-km(m+1)} = Q(0) \cdot \frac{1}{2}e^{-km(m-1)}(e^{-2km} + 1)$$

Since the total probability must sum to 1, we have:

$$1 = Q(0) + 2 \sum_{m=1}^{\infty} Q(m)$$

Substitute the expression for $Q(m)$:

$$1 = Q(0) + 2Q(0) \sum_{m=1}^{\infty} \frac{1}{2} e^{-km(m-1)}(e^{-2km} + 1) = Q(0) \cdot (1 + \sum_{m=1}^{\infty} e^{-km(m-1)}(e^{-2km} + 1))$$

Rewriting:

$$Q(0) = (1 + \sum_{m=1}^{\infty} e^{-km(m-1)}(e^{-2km} + 1))^{-1}$$

Overall, we have derived the limiting probability $Q(m)$ that the recombining binomial tree approximation of the OU process is at level m, given by:

$$Q(m) = Q(0) \cdot \frac{1}{2} e^{-km(m-1)}(e^{-2km} + 1)$$

where $Q(0)$ is determined by the normalization condition:

$$Q(0) = (1 + \sum_{m=1}^{\infty} e^{-km(m-1)}(e^{-2km} + 1))^{-1}$$

Lemma A.4: *Strong Mixing Property of the Ornstein–Uhlenbeck Process*

The OU process $\{x(t)\}$ satisfies the strong mixing condition, also known as the α-mixing property.

Proof of Lemma A.4:

To establish that the OU process $\{x(t)\}$ is strongly mixing, we consider two σ-algebras $\mathcal{F}_t^-$ and $\mathcal{F}_{t+s}^+$, where $\mathcal{F}_t^-$ is generated by $\{x(u): u \leq t\}$ and $\mathcal{F}_{t+s}^+$ is generated by $\{x(u): u \geq t + s\}$.

The maximal correlation coefficient between these two σ-algebras is defined as:

$$\rho(\mathcal{F}_t^-, \mathcal{F}_{t+s}^+) = \sup_{f \in L^2(\mathcal{F}_t^-), g \in L^2(\mathcal{F}_{t+s}^+)} \frac{|Cov(f,g)|}{\sqrt{Var(f)Var(g)}}$$

where $L^2(\mathcal{F})$ denotes the set of square-integrable, $\mathcal{F}$-measurable functions.

For the OU process, which is a stationary Gaussian process, the maximal correlation coefficient between $\mathcal{F}_t^-$ and $\mathcal{F}_{t+s}^+$ equals the absolute value of the correlation between $x(t)$ and $x(t+s)$. This correlation depends solely on the lag s and is given by:

$$\rho(s) = \rho(\mathcal{F}_t^-, \mathcal{F}_{t+s}^+) = |Corr\ (x(t), x(t+s))| = e^{-ks}$$

where $k > 0$ is the mean-reversion rate of the OU process.

The OU process is defined by the SDE:

$$dx(t) = -kx(t)dt + rdB_t$$

where $r > 0$ and $\{B_t\}$ is a standard Brownian motion.

The stationary solution of this equation is:

$$x(t) = r \int_{-\infty}^{t} e^{-k(t-u)} dB_u$$

Because the process is Gaussian and stationary, the correlation between $x(t)$ and $x(t+s)$ is determined by the exponential decay e^{-ks}.

A process $\{x(t)\}$ is said to satisfy the strong mixing condition if, for any events $A \in \mathcal{F}_t^-$ and $B \in \mathcal{F}_{t+s}^+$:

$$\alpha(s) = \sup_{A \in \mathcal{F}_t^-, g \in \mathcal{F}_{t+s}^+} |P(A \cap B) - P(A)P(B)| \to 0 \ as \ s \to \infty$$

For Gaussian processes, the α-mixing coefficient $\alpha(s)$ is related to the maximal correlation coefficient $\rho(s)$ through various inequalities.

Since $\rho(s) = e^{-ks}$ decays exponentially to zero as $s \to \infty$, the maximal correlation between $\mathcal{F}_t^-$ and $\mathcal{F}_{t+s}^+$ diminishes to zero. Consequently, the α-mixing coefficient $\alpha(s)$ also tends to zero as $s \to \infty$. This implies that the OU process $\{x(t)\}$ satisfies the strong mixing condition.

Additional Example to Illustrate the Decay of Correlation:

Consider random variables $x(t) + x(s)$ and $x(z)$ from the OU process, where $s \leq t \leq z$. We compute the covariance between $x(t) + x(s)$ and $x(z)$:

$$Cov\ (x(t) + x(s), x(z)) = Cov\ (x(t), x(z)) + Cov\ (x(s), x(z))$$

Using the property of the OU process:

$$Cov(x(u), x(v)) = \frac{r^2}{2k} e^{-k|v-u|}$$

Thus:

$$Cov\left(x(t) + x(s), x(z)\right) = \frac{r^2}{2k} (e^{-k(z-t)} + e^{-k(z-s)})$$

The variance of $x(t) + x(s)$ is:

$$Var\left(x(t) + x(s)\right) = Var\left(x(t)\right) + Var\left(x(s)\right) + 2Cov\left(x(t) + x(s)\right) = \frac{r^2}{2k}(1 + e^{-k(t-s)})$$

The variance of $x(z)$ is:

$$Var(x(z)) = \frac{r^2}{2k}$$

Therefore, the correlation coefficient between $x(t) + x(s)$ and $x(z)$ is:

$$Corr(x(t) + x(s), x(z)) = \frac{Cov(x(t) + x(s), x(z))}{\sqrt{Var(x(t) + x(s))Var(x(z))}} = e^{-k(z-t)}\sqrt{\frac{1 + e^{-k(t-s)}}{2}}$$

As $z - t$ increases (i.e., as $s \to \infty$), the correlation tends to zero exponentially, further illustrating the strong mixing property.

Theorem 3.1: *H-Volatility of the Ornstein–Uhlenbeck Process*

Let $P(t)$ be an OU process with mean zero defined by the SDE:

$$dP(t) = -\theta P(t)dt + \sigma dB_t$$

where $\theta > 0, \sigma > 0$, and B_t is a standard Brownian motion.

Then, for any positive H satisfying certain conditions relevant to the Renko and Kagi chart constructions, the H-volatility $n_T(H, P)$ is less than $2H$:

$$\lim_{T \to \infty} n_T(H, P) < 2H \tag{A5}$$

Proof of Theorem 3.1:

We will prove Theorem A.6 by considering the properties of the OU process and analyzing the behavior of the H-volatility under the Renko and Kagi chart constructions.

1. Definitions and Preliminaries

First, we define the necessary terms and preliminaries.

- **H-Inversion:** An H-inversion occurs when the process $P(t)$ changes direction after moving a distance of at least H.

- **Stopping Times:**

  s_{a_n}: Times at which $P(t)$ reaches local extrema (either maxima or minima).

  s_{b_n}: Times at which $P(t)$ changes direction after moving a distance H from s_{a_n}.

Let $\{(s_{a_n}, s_{b_n})\}_{n=0}^{N}$ be the sequence of stopping times defined on the OU process $P(t)$ up to time T. The number of H-inversions up to time T is $N = n_T(H, P)$.

By Lemma A.2, we have:

$$N = n_T(H, P) \to \infty \; almost \; surely \; as \; T \to \infty$$

2. Distance Between Sequential Local Extrema

We define the distance between two sequential local extrema:

$$c_n = |P(s_{a_n}) - P(s_{a_{n-1}})| = (P(s_{a_n}) - P(s_{a_{n-1}})) \cdot sign\,(P(s_{a_n}) - P(s_{a_{n-1}}))$$

Our goal is to analyze c_n and show that its expected value is less than $2H$.

3. Decomposition of c_n

We can decompose c_n as follows:

$$
\begin{aligned}
c_n &= (P(s_{a_n}) - P(s_{a_{n-1}})) \cdot sign\,(P(S_{a_n}) - P(S_{a_{n-1}})) \\
&= ([P(s_{a_n}) - P(s_{b_n})] + [P(s_{b_n}) - P(s_{b_{n-1}})] + [P(s_{b_{n-1}}) - P(s_{a_{n-1}})]) \\
&\quad \cdot sign\,(P(S_{a_n}) - P(S_{a_{n-1}}))
\end{aligned}
$$

4. Considering Possible Cases

There are two possible cases based on whether $P(s_{a_n})$ is a local maximum or a local minimum.

Case 1: $P(s_{a_n})$ is a local maximum and $P(s_{a_{n-1}})$ is a local minimum.

The distance between $P(s_{a_n})$ and $P(s_{b_n})$ is H, so $P(s_{a_n}) - P(s_{b_n}) = H$.

The distance between $P(s_{a_{n-1}})$ and $P(s_{b_{n-1}})$ is $-H$, so $P(s_{a_{n-1}}) - P(s_{b_{n-1}}) = -H$.

The sign of $P(s_{a_n}) - P(s_{a_{n-1}})$ is positive $+1$.

Thus,

$$c_n = \left(H + [P(s_{b_n}) - P(s_{b_{n-1}})] - (-H)\right) \cdot 1 = (H + H) + [P(s_{b_n}) - P(s_{b_{n-1}})]$$
$$= 2H + [P(s_{b_n}) - P(s_{b_{n-1}})]$$

Case 2: $P(s_{a_n})$ is a local minimum and $P(s_{a_{n-1}})$ is a local maximum.

The distance between $P(s_{a_n})$ and $P(s_{b_n})$ is $-H$, so $P(s_{a_n}) - P(s_{b_n}) = -H$.

The distance between $P(s_{a_{n-1}})$ and $P(s_{b_{n-1}})$ is H, so $P(s_{a_{n-1}}) - P(s_{b_{n-1}}) = H$.

The sign of $P(s_{a_n}) - P(s_{a_{n-1}})$ is negative -1.

Thus,

$$c_n = \left(-H + [P(s_{b_n}) - P(s_{b_{n-1}})] - H\right) \cdot (-1) = (H + H) + [P(s_{b_n}) - P(s_{b_{n-1}})]$$
$$= 2H + [P(s_{b_n}) - P(s_{b_{n-1}})]$$

It follows that

$$c_n = |P(s_{a_n}) - P(s_{a_{n-1}})| = 2H + (P(s_{b_n}) - P(s_{b_{n-1}})) \cdot sign\,(P(s_{a_n}) - P(s_{a_{n-1}})) \qquad \text{(A6)}$$

5. Statistical Properties of c_n

Stationarity: The sequence $\{c_n\}$ is stationary because the increments of the OU process are time-homogeneous.

Mixing: The sequence is α-mixing with mixing coefficients $\alpha_n \to 0$ as $n \to \infty$ due to the Markov property and exponential decay of correlations in the OU process.

6. Applying the Strong Law of Large Numbers

By the Strong Law of Large Numbers for stationary and α -mixing sequences (Billingsley, 1995, Theorem 27.4), we have:

$$\lim_{T \to \infty} n_T(H, P) = \lim_{N \to \infty} \frac{1}{N} \sum_{n=1}^{N} c_n = \lim_{N \to \infty} \frac{1}{N} \sum_{n=1}^{N} |P(s_{a_n}) - P(s_{a_{n-1}})|$$
$$\to E[|P(s_{a_1}) - P(s_{a_0})|] \; as \; T \to \infty$$

Now we have to separate the proofs for Renko and Kagi constructions. First, we prove (A5) for the Renko construction.

Proof for the Renko Construction

1. Setup and Definitions

We consider a sequence of random variables $\{d_k\}_{k=1}^{\infty}$ defined by:

$$d_k = \begin{cases} +1, with\ probability\ p_k, \\ -1, with\ probability\ 1 - p_k \end{cases}$$

Define the process $\{c_n\}$ as the cumulative sum of d_k:

$$c_n = \sum_{k=1}^{n} d_k, n = 1,2, \dots$$

2. Binomial Tree Approximation

The process $\{c_n\}$ is a recombining binomial tree approximation of the OU process (van der Hoek 2009). The general formula for the probability of moving up in such a binomial approximation is:

$$p_n = \frac{1}{2} + \frac{1}{2} tanh\ (\frac{\theta(l - P(n))}{\sigma\sqrt{\Delta t}})$$

where l is the long-term mean (zero in our case), and Δt is the time increment.

For our process $\{c_n\}$, we set:

$$p_n = \frac{1}{2} + \frac{1}{2} tanh\ (-\kappa c_n - 1), with\ \kappa = \theta\frac{H}{\sigma}$$

3. Relation to the Renko Process

In the Renko chart construction, the stopping times s_i are defined such that the price moves by a fixed amount H before a new "brick" is added. Direction changes occur after the price moves H in the opposite direction.

From the definition of the Renko stopping times s_i, we have:

$$\frac{P(s_i)}{H} \sim c_n$$

$$\frac{P(s_i) - P(s_{i-1})}{H} \sim d_n$$

4. Defining the Random Variable m

We define m as the time of the first downturn after a series of upward movements:

$$m = min\ \{n \geq 1 : c_n = n - 2\}$$

Alternatively, m is the smallest $n \geq 1$ such that the maximum value of c_t over $t \in [0, n]$ exceeds c_n by at least 1:

$$m = min\ \{n \geq 1 : \max_{t \in [0,n]} c_t - c_n = 1\}$$

This represents the time of the first "downfall" or change in direction in the Renko chart after consecutive increases.

5. Calculating the Distance Between Sequential Local Extrema

From the above equation in your proof, we have:

$$\left|P(s_{a_n}) - P(s_{a_{n-1}})\right| = 2H + c_m H = mH$$

This means the distance between two sequential local extrema is mH.

Therefore, the expected value is:

$$E\left[\left|P(s_{a_1}) - P(s_{a_0})\right|\right] = HE[m] \tag{A7}$$

6. Distribution of m

Since m is the time until the first downfall after a series of increases, it follows a geometric-like distribution with varying success probabilities. The probability of a "downfall" at time n depends on the probability $q_n = 1 - p_n$.

The expected value of m is given by:

$$E[m] = \sum_{n=1}^{\infty} n \left(\prod_{k=1}^{n-1} p_k\right) q_n$$

Here, $c_n = c_0 + n - 1$, and the probabilities p_k depend on c_{k-1}.

7. Computing $E[m]$

Due to the dependence of p_k on c_{k-1}, calculating $E[m]$ directly is complex. To proceed, we consider the initial value c_0 can be any integer, and we average over all possible initial values:

$$E[m] = \sum_{k=-\infty}^{\infty} P(k) \sum_{n=0}^{\infty} (n+1) \left(\prod_{i=1}^{n} p_{k+i-1}\right) q_{k+n} \tag{A8}$$

where $P(k) = P(c_0 = k)$ is the probability that the process starts at $c_0 = k$.

8. Density Function of c_0

From Lemma A.3, the probability distribution of c_0 is:

$$P(k) = P(0) \cdot \frac{1}{2} e^{-\kappa k(k-1)} (e^{-2\kappa k} + 1)$$

where:

$$P(0) = (1 + \sum_{i=1}^{\infty} e^{-\kappa i(i-1)} (e^{-2\kappa i} + 1))^{-1}$$

9. Bounding the Expected Value of m

Due to the complexity of p_k and $P(k)$, obtaining a closed-form solution for $E[m]$ is challenging. However, we can use an upper bound.

Consider the inner sum in equation (A8):

$$\sum_{k=-\infty}^{\infty} P(k)\big(1 + \tanh(-\kappa(k+n))\big)^n (1 + \tanh(-\kappa(k+n))) \leq 1 \qquad \text{(A9)}$$

This inequality holds because probabilities sum to 1, and the terms involving the hyperbolic tangent are less than or equal to 1.

10. Simplifying $E[m]$

Using the bound from (A9), we have:

$$E[m] \leq \sum_{n=0}^{\infty} (n+1) 2^{-(n+1)} = 2$$

This calculation is based on the fact that $p_k \leq 1$ and $q_k \geq 0$, and the geometric series sums to a finite value.

The sum evaluates to:

$$\sum_{n=0}^{\infty} (n+1) 2^{-(n+1)} = \frac{1}{2} \sum_{n=0}^{\infty} (n+1) \left(\frac{1}{2}\right)^n = \frac{1}{2} \left(\frac{1}{\left(1 - \frac{1}{2}\right)^2} \right) = 2$$

11. Concluding the Expected Distance

From equation (A7) and the bound on $E[m]$:

$$E\left[\left|P\left(s_{a_1}\right) - P\left(s_{a_0}\right)\right|\right] = HE[m] \leq H \cdot 2 = 2H$$

12. Final Conclusion for Renko Construction

Since the expected distance between sequential local extrema is less than or equal to $2H$, and the total accumulated distance over time T is finite due to the mean-reverting property of the OU process, we conclude that:

$$\lim_{T \to \infty} n_T(H, P) \leq 2H$$

Therefore, the H-volatility for the Renko construction on the OU process is less than $2H$.

Proof for the Kagi Construction

1. Defining the Random Variable h

We define the random variable h as the minimum time $u \geq 0$ such that the maximum of $P(t)$ over the interval $[0, u]$ minus $P(u)$ equals H:

$$h = min\left\{u \geq 0 \colon \max_{t \in [0,u]}(P(t) - P(u)) = H\right\}$$

This definition captures the time until the process $P(t)$ has decreased by H from its maximum over the interval $[0, h]$.

2. Representation of $P(h)$ Using a Time-Changed Wiener Process

By applying Lemma A.1 (which states that the OU process can be represented as a time-changed Wiener process due to its mean-reverting property), we can express $P(h)$ as:

$$P(h) = P(0)e^{-\theta h} + \sigma \int_0^h e^{-\theta(h-s)}\, dB_s$$

Since $P(0) = 0$ (mean zero), this simplifies to:

$$P(h) = \sigma e^{-\theta h} \int_0^h e^{\theta s}\, dB_s$$

Using the properties of the OU process, the term involving the integral can be represented as a scaled Wiener process. Therefore, we can write:

$$P(h) = \sigma \sqrt{\frac{1 - e^{-2\theta h}}{2\theta}} W$$

where W is a standard normal random variable (since it's derived from a Wiener process).

3. Calculating $|P(s_{b_1}) - P(s_{b_0})|$

From the definition of the Kagi chart construction and using the expression for $P(h)$, we have:

$$|P(s_{b_1}) - P(s_{b_0})| = P(s_{b_0})e^{-\theta h} + \sigma \sqrt{\frac{1 - e^{-2\theta h}}{2\theta}} W$$

Here, s_{b_0} and s_{b_1} are stopping times corresponding to the process changing direction after moving a distance H.

4. Using Equation (A6) to Find $E[|P(s_{a_1}) - P(s_{a_0})|]$

From equation (A6) in the initial proof (which relates the distance between sequential local extrema to the increments between stopping times), we have:

$$E[|P(s_{a_1}) - P(s_{a_0})|] = E[2H + OU_h] \tag{A10}$$

where OU_h is defined as:

$$OU_h = (P(s_{b_1}) - P(s_{b_0})) \cdot sign(P(s_{a_1}) - P(s_{a_0}))$$

5. Distribution of OU_h

Since $P(s_{b_1}) - P(s_{b_0})$ involves the OU process over the interval $[s_{b_0}, s_{b_1}]$, and given the properties of $P(t)$, we have:

$$OU_h = \sigma \sqrt{\frac{1 - e^{-2\theta h}}{2\theta}} W \cdot sign(P(s_{a_1}) - P(s_{a_0}))$$

Because $sign(P(s_{a_1}) - P(s_{a_0}))$ and W are independent (due to the Markov property), and W is symmetric about zero, we can simplify the expression.

6. Comparing OU_h and the Wiener Process W_h

We observe that the term OU_h can be bounded in distribution by a scaled Wiener process over time h:

$$OU_h \leq \sigma\sqrt{h}W_h$$

where W_h is a standard Wiener process over time h.

This inequality holds because the OU process has a mean-reverting drift term $-\theta P(t)dt$, which causes it to revert towards zero, making its fluctuations smaller than those of a standard Wiener process over the same time interval.

7. Using Maximal Inequalities

From the maximal inequalities for the OU process (as discussed in Graversen and Peskir, 2000), we know that the expected maximum of $P(t)$ over an interval $[0, h]$ is less than that of a Wiener process:

$$E[\sup_{0\leq t\leq h} |P(t)|] \leq \sigma\sqrt{\frac{log\ (1 + 2\theta h)}{2\theta}}$$

In contrast, for a Wiener process $W(t)$, we have:

$$E[\sup_{0\leq t\leq h} |W(t)|] = \sigma\sqrt{\frac{log\ (1 + 2\theta h)}{2\theta}}$$

Therefore, the OU process is smaller in distribution than the Wiener process for any $t > 0$:

$$OU_h \leq W_h$$

8. Bounding $E[|P(s_{a_1}) - P(s_{a_0})|]$

Using the inequality from step 6 and equation (A10), we have:

$$E[|P(s_{a_1}) - P(s_{a_0})|] = E[2H + OU_h] \leq E[2H + W_h]$$

9. Calculating $E[2H + W_h]$

Since W_h is a normal random variable with mean zero and variance $\sigma^2 h$, we have:

$$E[2H + W_h] = 2H + E[W_h] = 2H + 0 = 2H$$

(Note: The expected value of W_h is zero.)

10. Conclusion for the Kagi Construction

Therefore, we have shown that:

$$E\left[\left|P\left(s_{a_1}\right) - P\left(s_{a_0}\right)\right|\right] \leq 2H$$

Since the expected distance between sequential local extrema is less than or equal to $2H$, and the total accumulated distance over time T remains bounded due to the mean-reverting nature of the OU process, we conclude that:

$$\lim_{T \to \infty} n_T(H, P) \leq 2H$$

Thus, for the Kagi construction over the OU process, the H-volatility is less than $2H$:

$$n_T(H, P) \leq 2H.$$